January 2005 • NREL/SR-500-36334

Subcontractor Report

The S819, S820, and S821 Airfoils

October 1992 – November 1993

D.M. Somers
Airfoils, Inc.
State College, Pennsylvania

National Renewable Energy Laboratory
1617 Cole Boulevard, Golden, Colorado 80401-3393
303-275-3000 • www.nrel.gov

Operated for the U.S. Department of Energy
Office of Energy Efficiency and Renewable Energy
by Midwest Research Institute • Battelle

Contract No. DE-AC36-99-GO10337

January 2005 • NREL/SR-500-36334

The S819, S820, and S821 Airfoils

October 1992 – November 1993

D.M. Somers
Airfoils, Inc.
State College, Pennsylvania

NREL Technical Monitor: Jim Tangler

Prepared under Subcontract No. AF-1-11154-1

National Renewable Energy Laboratory
1617 Cole Boulevard, Golden, Colorado 80401-3393
303-275-3000 • www.nrel.gov

Operated for the U.S. Department of Energy
Office of Energy Efficiency and Renewable Energy
by Midwest Research Institute • Battelle

Contract No. DE-AC36-99-GO10337

Available electronically at http://www.osti.gov/bridge

Available for a processing fee to U.S. Department of Energy
and its contractors, in paper, from:
U.S. Department of Energy
Office of Scientific and Technical Information
P.O. Box 62
Oak Ridge, TN 37831-0062
phone: 865.576.8401
fax: 865.576.5728
email: mailto:reports@adonis.osti.gov

Available for sale to the public, in paper, from:
U.S. Department of Commerce
National Technical Information Service
5285 Port Royal Road
Springfield, VA 22161
phone: 800.553.6847
fax: 703.605.6900
email: orders@ntis.fedworld.gov
online ordering: http://www.ntis.gov/ordering.htm

Printed on paper containing at least 50% wastepaper, including 20% postconsumer waste

Table of Contents

List of Tables

List of Figures

THE S819, S820, AND S821 AIRFOILS

Dan M. Somers

November 1993

ABSTRACT

A family of thick airfoils for 10- to 20-meter, stall-regulated, horizontal-axis wind turbines, the S819, S820, and S821, has been designed and analyzed theoretically. The primary objectives of restrained maximum lift, insensitive to roughness, and low profile drag have been achieved. The constraints on the pitching moments and airfoil thicknesses have been satisfied.

INTRODUCTION

The family of thick airfoils designed under this study is intended for 10- to 20-meter, stall-regulated, horizontal-axis wind turbines. Two earlier thick-airfoil families, the S809, S810, and S811 (ref. 1) and the S816, S817, and S818 (ref. 2), were designed for 20- to 30-meter and 30- to 40-meter wind turbines, respectively.

The specific tasks performed under this study are described in National Renewable Energy Laboratory (NREL) Subcontract Number AAO-3-13023-01-104879. The specifications for the airfoils are outlined in the Statement of Work.

Because of the limitations of the theoretical methods (refs. 3 and 4) employed in this study, the results presented are in no way guaranteed to be accurate—either in an absolute or in a relative sense. This statement applies to the entire study.

SYMBOLS

C_p	pressure coefficient
c	airfoil chord, meters
c_d	section profile-drag coefficient
c_l	section lift coefficient

c_m	section pitching-moment coefficient about quarter-chord point
L.	lower surface
MU	boundary-layer transition mode (ref. 4)
R	Reynolds number based on free-stream conditions and airfoil chord
S.	boundary-layer separation location, $1 - s_{sep}/c$
s_{sep}	arc length along which boundary layer is separated, meters
s_{turb}	arc length along which boundary layer is turbulent including s_{sep}, meters
T.	boundary-layer transition location, $1 - s_{turb}/c$
U.	upper surface
x	airfoil abscissa, meters
y	airfoil ordinate, meters
α	angle of attack relative to chord line, degrees

AIRFOIL DESIGN

OBJECTIVES AND CONSTRAINTS

The design specifications for the family of airfoils are contained in table I. The family consists of three airfoils, primary, tip, and root, corresponding to the 0.75, 0.95, and 0.40 blade radial stations, respectively.

Two primary objectives are evident from the specifications. The first objective is to restrain the maximum lift coefficients of the primary and tip airfoils to relatively low values. In contrast, the maximum lift coefficient of the root airfoil should be as high as possible. A requirement related to this objective is that the maximum lift coefficient not decrease with transition fixed near the leading edge on both surfaces. The second objective is to obtain low profile-drag coefficients over the ranges of lift coefficients from 0.4 to 1.0 for the primary airfoil, from 0.3 to 0.9 for the tip airfoil, and from 0.6 to 1.2 for the root airfoil.

Two major constraints were placed on the designs of these airfoils. First, the zero-lift pitching-moment coefficients must be no more negative than −0.07 for the primary and tip airfoils and −0.15 for the root airfoil. Second, the airfoil thicknesses must equal 21-percent chord for the primary airfoil, 16-percent chord for the tip airfoil, and 24-percent chord for the root airfoil.

PHILOSOPHY

Given the above objectives and constraints, certain characteristics of the designs are evident. The following sketch illustrates a drag polar which meets the goals for these designs.

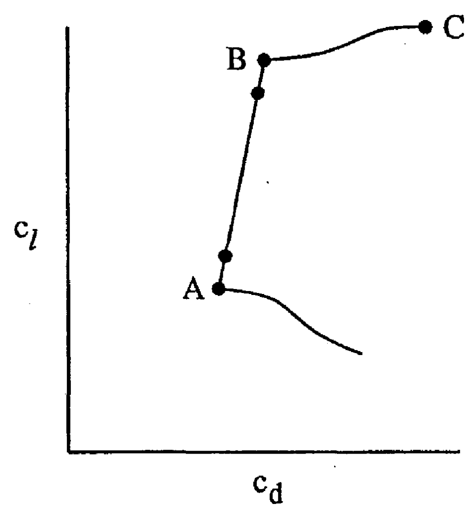

Sketch 1

The desired airfoil shapes can be traced to the pressure distributions which occur at the various points in sketch 1. Point A is the lower limit of the low-drag, lift-coefficient range. The lift coefficient at point A is 0.1 lower than the objective specified in table I. The difference is intended as a margin against such contingencies as manufacturing tolerances, operational deviations, three-dimensional effects, and inaccuracies in the theoretical method. A similar margin is also desirable at the upper limit of the low-drag, lift-coefficient range, point B. The drag at point B is not as low as at point A, unlike the polars of many laminar-flow airfoils where the drag within the laminar bucket is nearly constant. This characteristic is related to the elimination of significant (drag-producing) laminar separation bubbles on the upper surface (see ref. 5) and is acceptable because the ratio of the profile drag to the total drag of the wind-turbine blade decreases with increasing lift coefficient. The drag increases very rapidly outside the laminar bucket because the boundary-layer transition point moves quickly toward the leading edge. This feature results in a rather sharp leading edge which produces a suction peak at higher lift coefficients, which limits the maximum lift coefficient and ensures that transition on the upper surface will occur very near the leading edge. Thus, the maximum lift coefficient occurs with turbulent flow along the entire upper surface and, therefore, should be insensitive to roughness at the leading edge. Point C is the maximum lift coefficient.

From the preceding discussion, the pressure distributions along the polar can be deduced. The pressure distribution at point A for the primary airfoil should look something like sketch 2. (The pressure distributions for the tip and root airfoils should be qualitatively similar.)

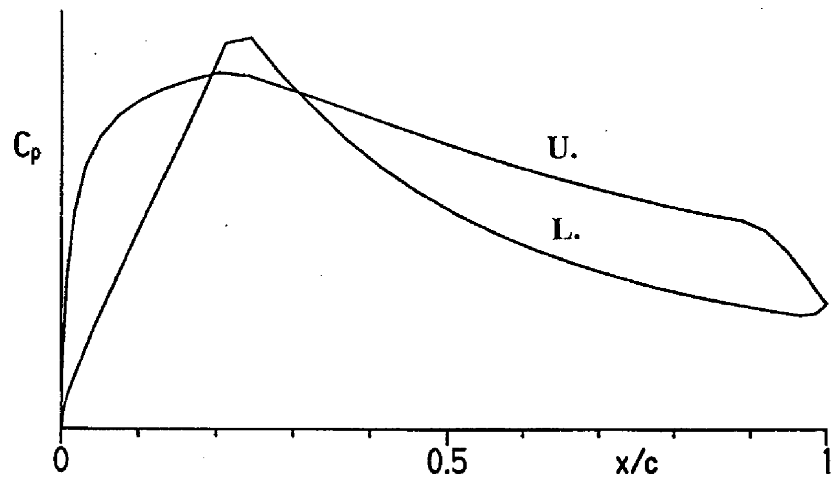

Sketch 2

To achieve low drag, a favorable pressure gradient is desirable along the upper surface to about 20-percent chord. Aft of this point, a short region having a shallow, adverse pressure gradient ("transition ramp") promotes the efficient transition from laminar to turbulent flow (ref. 6). This short region is followed by a steeper concave pressure recovery. The specific concave pressure recovery employed represents a compromise among maximum lift, low drag, and docile stall characteristics. The steep adverse pressure gradient on the upper surface aft of about 90-percent chord is a 'separation ramp,' originally proposed by F. X. Wortmann, which confines turbulent separation to a small region near the trailing edge. By controlling the movement of the separation point at high angles of attack, high lift coefficients can be achieved with little drag penalty. This feature has the added benefit that it promotes docile stall characteristics. (See ref. 7.)

A favorable pressure gradient is desirable along the lower surface to about 25-percent chord to achieve low drag. The pressure gradients along the forward portion of the lower surface increase the amount of camber in the leading-edge region while maintaining low drag at the lower limit of the laminar bucket. The forward camber serves to balance, with respect to the pitching-moment constraint, the aft camber, both of which contribute to the achievement of the maximum lift coefficient. This region is followed by a curved transition ramp (ref. 5) which is longer than that on the upper surface. The transition ramp is followed by a concave pressure recovery which exhibits lower drag and has less tendency to separate than the corresponding linear or convex pressure recovery. The pressure recovery must begin relatively far forward to alleviate lower-surface separation at lower lift coefficients.

The amounts of pressure recovery on the two surfaces are determined by the airfoil-thickness and pitching-moment constraints.

At point B, the pressure distribution should look like sketch 3.

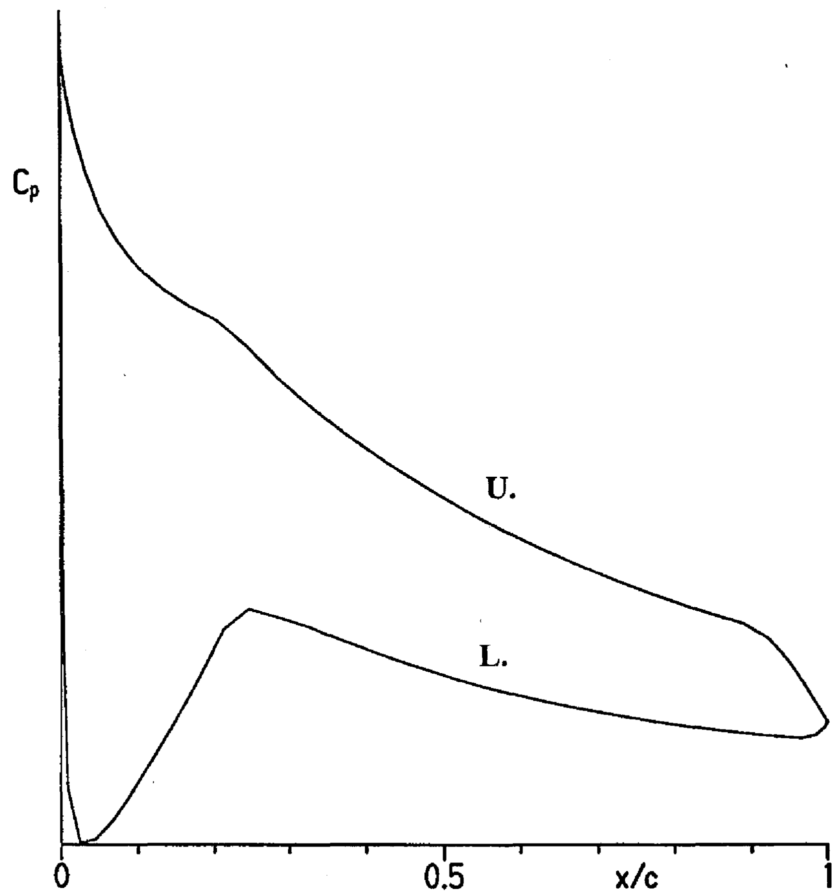

Sketch 3

A severe suction spike does not exist at the leading edge because of the incorporation of increasingly favorable pressure gradients toward the leading edge. This feature allows a wider laminar bucket to be achieved and higher lift coefficients to be reached without significant separation.

EXECUTION

Given the pressure distributions previously discussed, the design of the airfoils is reduced to the inverse problem of transforming the pressure distributions into airfoil shapes. The Eppler Airfoil Design and Analysis Code (refs. 3 and 4) was used because of confidence gained during the design, analysis, and experimental verification of several other airfoils. (See refs. 8–10.)

The primary airfoil is designated the S819. The tip airfoil, the S820, and the root airfoil, the S821, were derived from the S819 airfoil to increase the aerodynamic and geometric compatibilities of the three airfoils. The airfoil shapes are shown in figure 1 and the coordinates are contained in tables II, III, and IV. The S819 airfoil thickness is 21-percent chord; the S820, 16-percent chord; and the S821, 24-percent chord.

DISCUSSION OF RESULTS

S819 AIRFOIL

Pressure Distributions

The inviscid (potential-flow) pressure distributions for the S819 airfoil for various angles of attack are shown in figure 2. Because the free-stream Mach number for all relevant operating conditions remains below 0.2, these and all subsequent results are incompressible.

Transition and Separation Locations

The variation of boundary-layer transition location with lift coefficient for the S819 airfoil is shown in figure 3. It should be remembered that the method of references 3 and 4 'defines' the transition location as the end of the laminar boundary layer whether due to natural transition or laminar separation. Thus, for conditions which result in relatively long laminar separation bubbles (low lift coefficients for the upper surface and high lift coefficients for the lower surface and/or low Reynolds numbers), poor agreement between the predicted 'transition' locations and the locations measured experimentally can be expected. This poor agreement is worsened by the fact that transition is normally confirmed in the wind tunnel only by the detection of attached turbulent flow. For conditions which result in shorter laminar separation bubbles (high lift coefficients for the upper surface and low lift coefficients for the lower surface and/or high Reynolds numbers), the agreement between theory and experiment should be quite good. (See ref. 11.)

The variation of turbulent boundary-layer separation location with lift coefficient for the S819 airfoil is shown in figure 3. A small separation is predicted on the upper surface at higher lift coefficients. This separation, which is caused by the separation ramp (fig. 2), increases in length with transition fixed near the leading edge. Separation is predicted on the lower surface at lift coefficients below about 0.1 with transition free and below about 0.4 with transition fixed for the design Reynolds number of 1.0×10^6. The lower-surface separation is not considered important because it occurs at lift coefficients which are not typical of normal wind-turbine operations. Also, such separation usually has little effect on the section characteristics. (See ref. 11.)

Section Characteristics

Reynolds number effects.- The section characteristics of the S819 airfoil are shown in figure 3. It should be noted that the maximum lift coefficient predicted by the method of references 3 and 4 is not always realistic. Accordingly, an empirical criterion should be applied to the computed results. This criterion assumes that the maximum lift coefficient has been reached if the drag coefficient of the upper surface is greater than 0.0240 or if the length of turbulent separation along the upper surface is greater than 0.10. Thus, the maximum lift coefficient for the design Reynolds number of 1.0×10^6 is predicted to be 1.20, which meets the design objective. Based on the movement of the upper-surface separation point, the stall characteristics are expected to be docile. Low profile-drag coefficients are predicted over the range of lift coefficients from about 0 to about 1.1, which exceeds the range specified (0.4 to 1.0). The drag coefficient at the specified lower limit of the laminar bucket ($c_l = 0.4$) is predicted to be 0.0097, which exceeds the design objective by 21 percent. The achievement of this objective was sacrificed to meet the other, more important objectives and constraints. The zero-lift pitching-moment coefficient is predicted to be –0.0778, which exceeds the design constraint. However, the method of references 3 and 4 generally overpredicts the pitching-moment coefficient by about 10 percent. Thus, the actual zero-lift pitching-moment coefficient should be about –0.07, which satisfies the constraint.

An additional analysis (not shown) indicates that significant (drag-producing) laminar separation bubbles should not occur on either surface for any relevant operating condition.

Effect of roughness.- The effect of roughness on the section characteristics of the S819 airfoil is shown in figure 3. Transition was fixed at 2-percent chord on the upper surface and 5-percent chord on the lower surface using transition mode MU = 1 (ref. 4). The maximum lift coefficient is unaffected by fixing transition at these locations because transition is predicted to occur forward of 2-percent chord on the upper surface at the maximum lift coefficient. The 'rough' results were obtained using transition mode MU = 9 (ref. 4), which simulates distributed roughness due to, for example, leading-edge contamination by insects or rain. At the higher lift coefficients, this transition mode is probably comparable to National Advisory Committee for Aeronautics (NACA) Standard Roughness which "is considerably more severe than that caused by the usual manufacturing irregularities or deterioration in service" (ref. 12). For the rough condition, the maximum lift coefficient for the design Reynolds number of 1.0×10^6 is predicted to be 1.16, a reduction of three percent from that for the transition-free condition. Thus, one of the most important design requirements has been achieved. The drag coefficients are, of course, adversely affected by the roughness.

S820 AIRFOIL

Pressure Distributions

The inviscid (potential-flow) pressure distributions for the S820 airfoil for various angles of attack are shown in figure 4.

Transition and Separation Locations

The variations of transition and turbulent-separation locations with lift coefficient for the S820 airfoil are shown in figure 5. A small separation is predicted on the upper surface at higher lift coefficients. This separation, which is caused by the separation ramp (fig. 4), increases in length with transition fixed near the leading edge.

Section Characteristics

Reynolds number effects.- The section characteristics of the S820 airfoil are shown in figure 5. Using the previously-described empirical criterion, the maximum lift coefficient for the design Reynolds number of 1.3×10^6 is predicted to be 1.10, which meets the design objective. The stall characteristics are expected to be docile. Low drag coefficients are predicted over the range of lift coefficients from about 0.1 to about 1.0, which exceeds the range specified (0.3 to 0.9). The drag coefficient at the specified lower limit of the laminar bucket ($c_l = 0.3$) is predicted to be 0.0060, which is 14 percent below the design objective. The zero-lift pitching-moment coefficient is predicted to be −0.0727, which exceeds the design constraint. Again, because the method of references 3 and 4 overpredicts the pitching-moment coefficient, the actual zero-lift pitching-moment coefficient should be about −0.07, which satisfies the constraint. Significant (drag-producing) laminar separation bubbles should not occur on either surface for any relevant operating condition.

Effect of roughness.- The effect of roughness on the section characteristics of the S820 airfoil is shown in figure 5. Transition was fixed at 2-percent chord on the upper surface and 5-percent chord on the lower surface using transition mode MU = 1. The maximum lift coefficient is essentially unaffected by fixing transition at these locations because transition is predicted to occur near 2-percent chord on the upper surface at the maximum lift coefficient. For the rough condition (MU = 9), the maximum lift coefficient for the design Reynolds number of 1.3×10^6 is predicted to be 1.06, a reduction of four percent from that for the transition-free condition. Thus, one of the most important design requirements has been achieved. The drag coefficients are, of course, adversely affected by the roughness.

S821 AIRFOIL

Pressure Distributions

The inviscid (potential-flow) pressure distributions for the S821 airfoil for various angles of attack are shown in figure 6.

Transition and Separation Locations

The variations of transition and turbulent-separation locations with lift coefficient for the S821 airfoil are shown in figure 7. A small separation is predicted on the upper surface at most lift coefficients. This separation, which is caused by the separation ramp (fig. 6), increases in length with transition fixed near the leading edge. Separation is predicted on the lower surface at lower lift coefficients. Such separation usually has only a minor effect on the section characteristics.

Section Characteristics

Reynolds number effects.- The section characteristics of the S821 airfoil are shown in figure 7. Using the previously-described criterion, the maximum lift coefficient for the design Reynolds number of 0.8×10^6 is predicted to be 1.40, which meets the design objective. The stall characteristics are expected to be docile. Low drag coefficients are predicted over the range of lift coefficients from 0 to about 1.1, which is wider but lower than the range specified (0.6 to 1.2) to meet the other, more important objectives and constraints. The drag coefficient at the specified lower limit of the laminar bucket ($c_l = 0.6$) is predicted to be 0.0117, which is 16 percent below the design objective. The zero-lift pitching-moment coefficient is predicted to be −0.1660, which exceeds the design constraint. Again, because the method of references 3 and 4 overpredicts the pitching-moment coefficient, the actual zero-lift pitching-moment coefficient should be about −0.15, which satisfies the constraint. Significant (drag-producing) laminar separation bubbles should not occur on either surface for any relevant operating condition.

Effect of roughness.- The effect of roughness on the section characteristics of the S821 airfoil is shown in figure 7. Transition was fixed at 2-percent chord on the upper surface and 5-percent chord on the lower surface using transition mode MU = 1. The maximum lift coefficient is unaffected by fixing transition at these locations because transition is predicted to occur forward of 2-percent chord on the upper surface at the maximum lift coefficient. For the rough condition (MU = 9), the maximum lift coefficient for the design Reynolds number of 0.8×10^6 is predicted to be 1.35, a reduction of four percent from that for the transition-free condition. Thus, one of the most important design requirements has been achieved. The drag coefficients are, of course, adversely affected by the roughness.

CONCLUDING REMARKS

A family of thick airfoils for 30- to 40-meter, stall-regulated, horizontal-axis wind turbines, the S819, S820, and S821, has been designed and analyzed theoretically. The primary objectives of restrained maximum lift coefficients, insensitive to roughness, and low profile-drag coefficients have been achieved. The constraints on the pitching-moment coefficients and airfoil thicknesses have been satisfied.

REFERENCES

1. Somers, Dan M.: The S809 through S813 Airfoils. Airfoils, Inc., 1988.

2. Somers, Dan M.: The S816, S817, and S818 Airfoils. Airfoils, Inc., 1992.

3. Eppler, Richard: Airfoil Design and Data. Springer-Verlag (Berlin), 1990.

4. Eppler, R.: Airfoil Program System. User's Guide. R. Eppler, c.1991.

5. Eppler, Richard; and Somers, Dan M.: Airfoil Design for Reynolds Numbers Between 50,000 and 500,000. Proceedings of the Conference on Low Reynolds Number Airfoil Aerodynamics, UNDAS-CP-77B123, Univ. of Notre Dame, June 1985, pp. 1–14.

6. Wortmann, F. X.: Experimental Investigations on New Laminar Profiles for Gliders and Helicopters. TIL/T.4906, British Minist. Aviat., Mar. 1960. (Translated from Z. Flugwissenschaften, Bd. 5, Heft 8, Aug. 1957, pp. 228–243.)

7. Maughmer, Mark D.; and Somers, Dan M.: Design and Experimental Results for a High-Altitude, Long-Endurance Airfoil. J. Aircr., vol. 26, no. 2, Feb. 1989, pp. 148–153.

8. Somers, Dan M.: Design and Experimental Results for the S809 Airfoil. Airfoils, Inc., 1989.

9. Somers, Dan M.: Design and Experimental Results for the S805 Airfoil. Airfoils, Inc., 1988.

10. Somers, Dan M.: Subsonic Natural-Laminar-Flow Airfoils. Natural Laminar Flow and Laminar Flow Control, R. W. Barnwell and M. Y. Hussaini, eds., Springer-Verlag New York, Inc., 1992, pp. 143–176.

11. Somers, Dan M.: Design and Experimental Results for a Natural-Laminar-Flow Airfoil for General Aviation Applications. NASA TP-1861, 1981.

12. Abbott, Ira H.; Von Doenhoff, Albert E.; and Stivers, Louis S., Jr.: Summary of Airfoil Data. NACA Rep. 824, 1945. (Supersedes NACA WR L-560.)

TABLE I.- AIRFOIL DESIGN SPECIFICATIONS

Parameter	Objective/Constraint		
Airfoil	Primary	Tip	Root
Blade radial station	0.75	0.95	0.40
Reynolds number	1.0×10^6	1.3×10^6	0.8×10^6
Maximum lift coefficient	1.20	1.10	1.40
Low-drag, lift-coefficient range:			
Lower limit	0.4	0.3	0.6
Upper limit	1.0	0.9	1.2
Minimum profile-drag coefficient	0.0080	0.0070	0.0140
Zero-lift pitching-moment coefficient	≥ -0.07	≥ -0.07	≥ -0.15
Thickness	0.21c	0.16c	0.24c

TABLE II.- S819 AIRFOIL COORDINATES

Upper Surface		Lower Surface	
x/c	y/c	x/c	y/c
0.00002	0.00077	0.00006	−0.00125
.00101	.00556	.00056	−.00298
.00673	.01572	.00177	−.00455
.01719	.02663	.00372	−.00622
.03213	.03768	.00891	−.00986
.05143	.04852	.02445	−.02021
.07486	.05890	.04415	−.03323
.10216	.06858	.06692	−.04746
.13302	.07733	.09234	−.06201
.16709	.08491	.11997	−.07614
.20398	.09099	.14948	−.08914
.24355	.09516	.18049	−.10033
.28581	.09736	.21265	−.10864
.33053	.09777	.24658	−.11280
.37732	.09651	.28355	−.11284
.42580	.09369	.32385	−.10966
.47552	.08949	.36718	−.10375
.52602	.08411	.41332	−.09557
.57678	.07780	.46189	−.08562
.62723	.07078	.51244	−.07440
.67679	.06331	.56446	−.06247
.72481	.05561	.61728	−.05039
.77067	.04792	.67018	−.03869
.81370	.04039	.72231	−.02789
.85327	.03316	.77274	−.01843
.88875	.02622	.82050	−.01064
.91979	.01940	.86454	−.00473
.94642	.01282	.90387	−.00075
.96851	.00712	.93753	.00141
.98545	.00295	.96464	.00197
.99626	.00066	.98437	.00136
1.00000	.00000	.99613	.00042
		1.00000	.00000

TABLE III.- S820 AIRFOIL COORDINATES

Upper Surface		Lower Surface	
x/c	y/c	x/c	y/c
0.00013	0.00133	0.00001	–0.00041
.00364	.00910	.00032	–.00178
.01172	.01811	.00117	–.00300
.02425	.02758	.00258	–.00423
.04120	.03708	.01207	–.00946
.06255	.04637	.02754	–.01514
.08815	.05531	.04834	–.02097
.11774	.06379	.07403	–.02684
.15102	.07167	.10419	–.03260
.18764	.07884	.13841	–.03813
.22719	.08520	.17622	–.04330
.26923	.09063	.21715	–.04798
.31330	.09501	.26072	–.05203
.35891	.09825	.30638	–.05533
.40555	.10022	.35360	–.05772
.45272	.10079	.40183	–.05903
.49988	.09978	.45050	–.05900
.54666	.09688	.49923	–.05721
.59300	.09196	.54807	–.05340
.63875	.08518	.59707	–.04785
.68373	.07668	.64604	–.04093
.72795	.06688	.69476	–.03316
.77109	.05656	.74277	–.02532
.81244	.04635	.78923	–.01803
.85123	.03666	.83325	–.01172
.88668	.02775	.87388	–.00668
.91818	.01962	.91020	–.00304
.94544	.01242	.94132	–.00077
.96806	.00661	.96644	.00029
.98531	.00263	.98490	.00047
.99624	.00057	.99620	.00020
1.00000	.00000	1.00000	.00000

TABLE IV.- S821 AIRFOIL COORDINATES

Upper Surface		Lower Surface	
x/c	y/c	x/c	y/c
0.00004	0.00203	0.00001	–0.00076
.00037	.00550	.00243	–.01654
.00110	.00874	.00887	–.03393
.00234	.01186	.01876	–.05219
.00405	.01499	.03170	–.07058
.01212	.02520	.04745	–.08838
.02684	.03773	.06576	–.10493
.04636	.04980	.08643	–.11944
.07040	.06118	.10959	–.13110
.09865	.07171	.13548	–.13943
.13075	.08122	.16433	–.14399
.16633	.08955	.19663	–.14462
.20495	.09652	.23262	–.14170
.24618	.10190	.27216	–.13552
.28970	.10538	.31514	–.12635
.33539	.10684	.36142	–.11455
.38300	.10642	.41081	–.10062
.43214	.10431	.46300	–.08518
.48234	.10066	.51756	–.06893
.53312	.09566	.57389	–.05266
.58396	.08955	.63119	–.03717
.63429	.08254	.68850	–.02322
.68353	.07489	.74465	–.01147
.73105	.06680	.79836	–.00239
.77624	.05851	.84823	.00376
.81848	.05016	.89291	.00700
.85715	.04192	.93109	.00763
.89164	.03377	.96165	.00615
.92166	.02552	.98346	.00340
.94740	.01733	.99601	.00093
.96886	.00996	1.00000	.00000
.98550	.00432		
.99625	.00102		
1.00000	.00000		

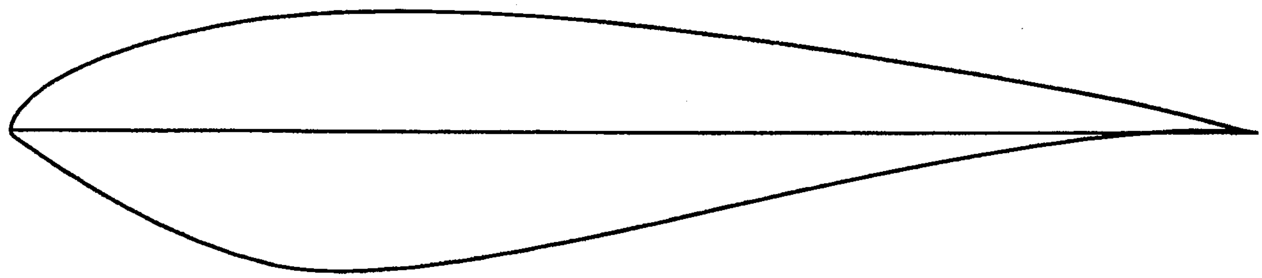

(a) S819.

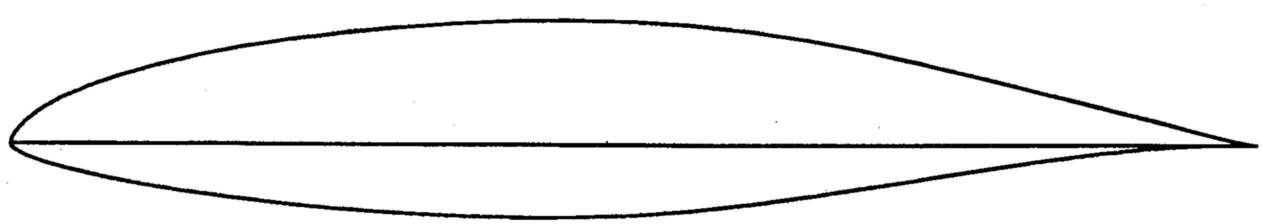

(b) S820.

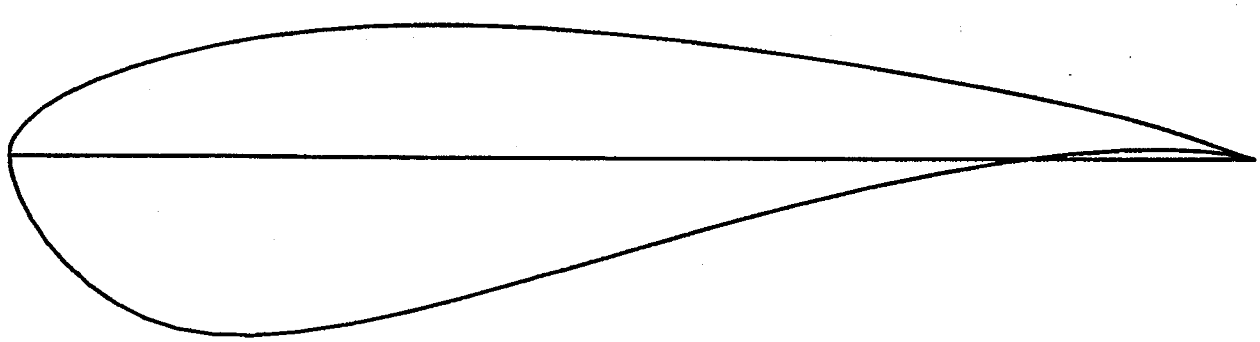

(c) S821.

Figure 1.- Airfoil shapes.

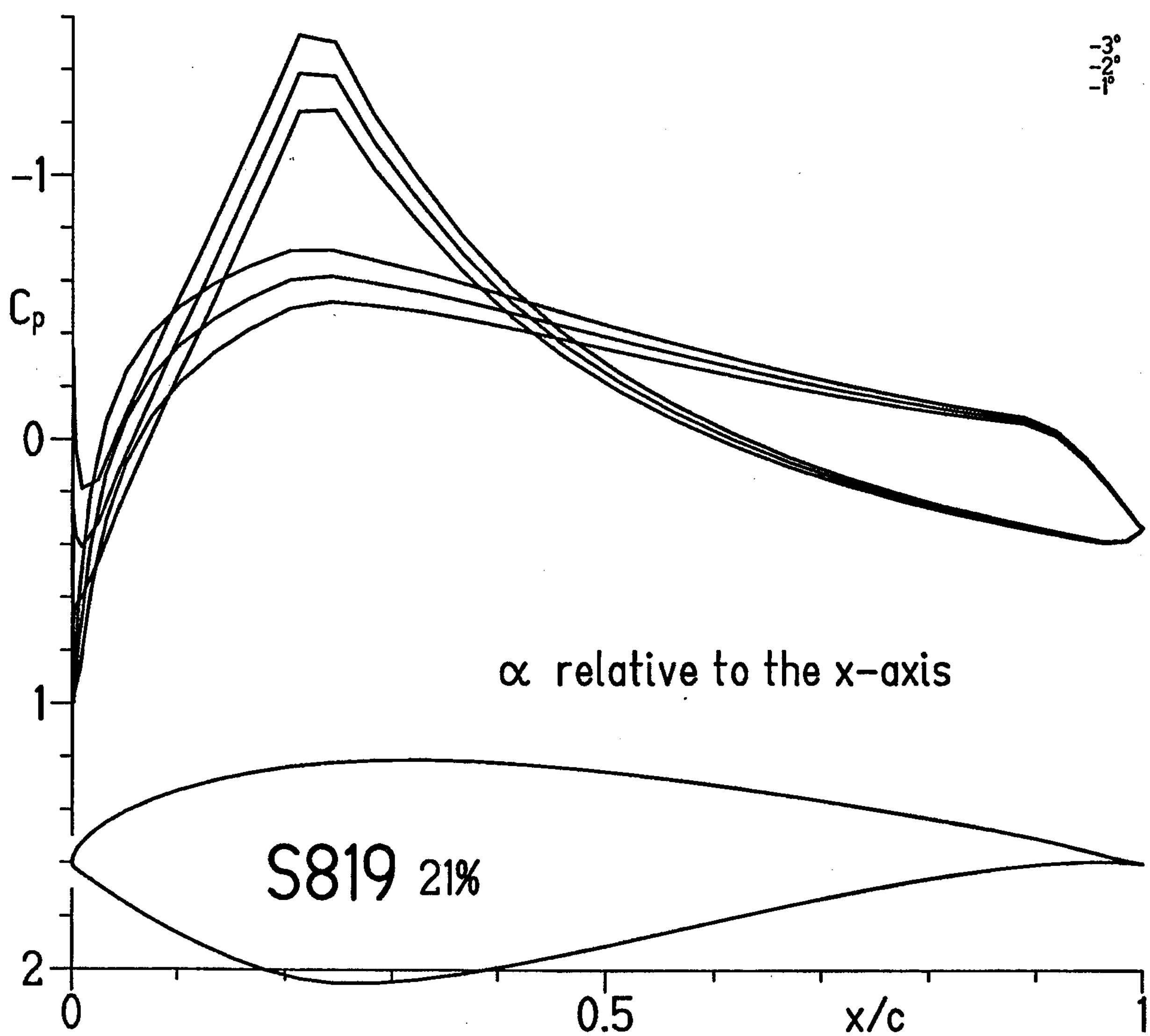

(a) α = –3°, –2°, and –1°.

Figure 2.- Inviscid pressure distributions for S819 airfoil.

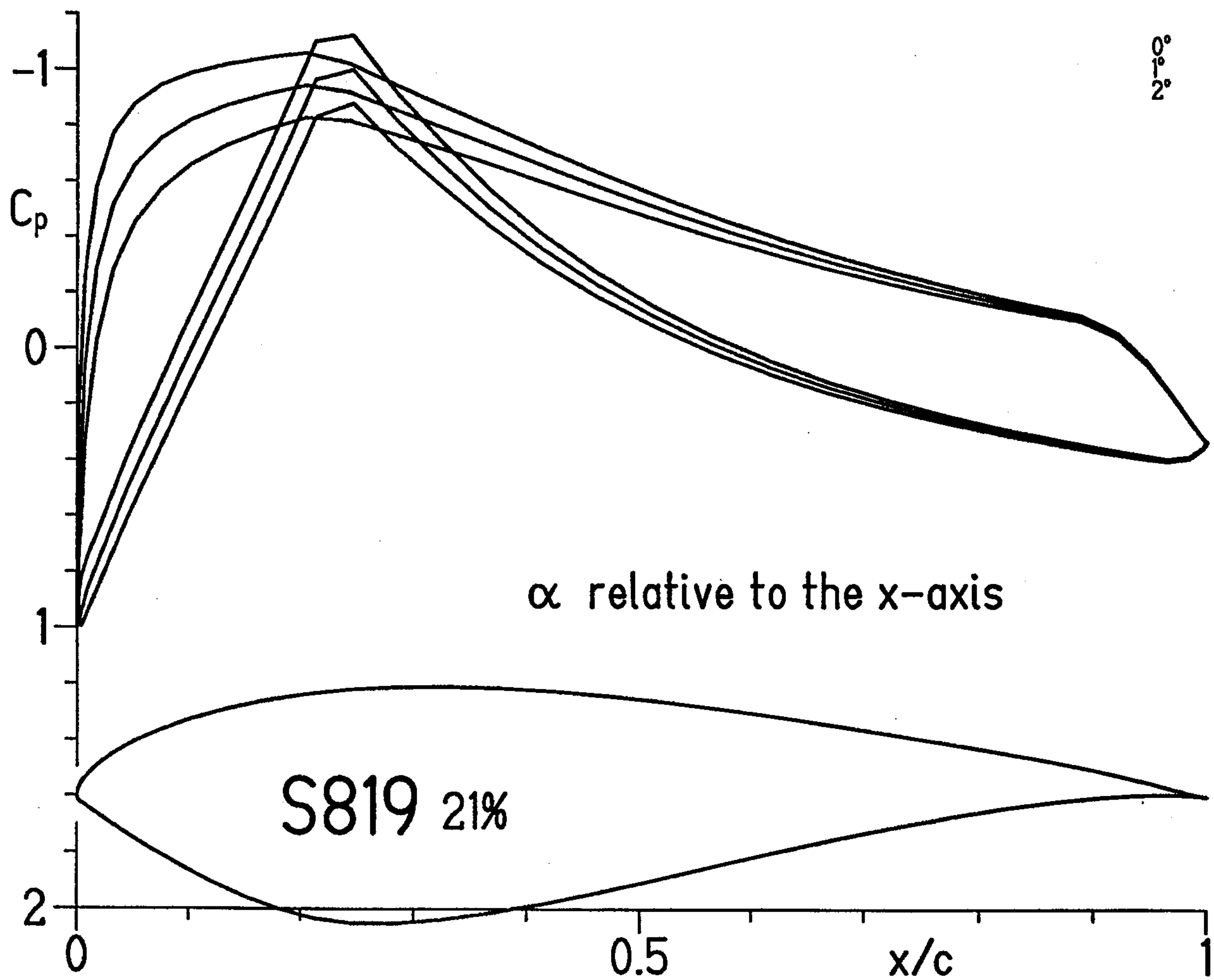

(b) α = 0°, 1°, and 2°.

Figure 2.- Continued.

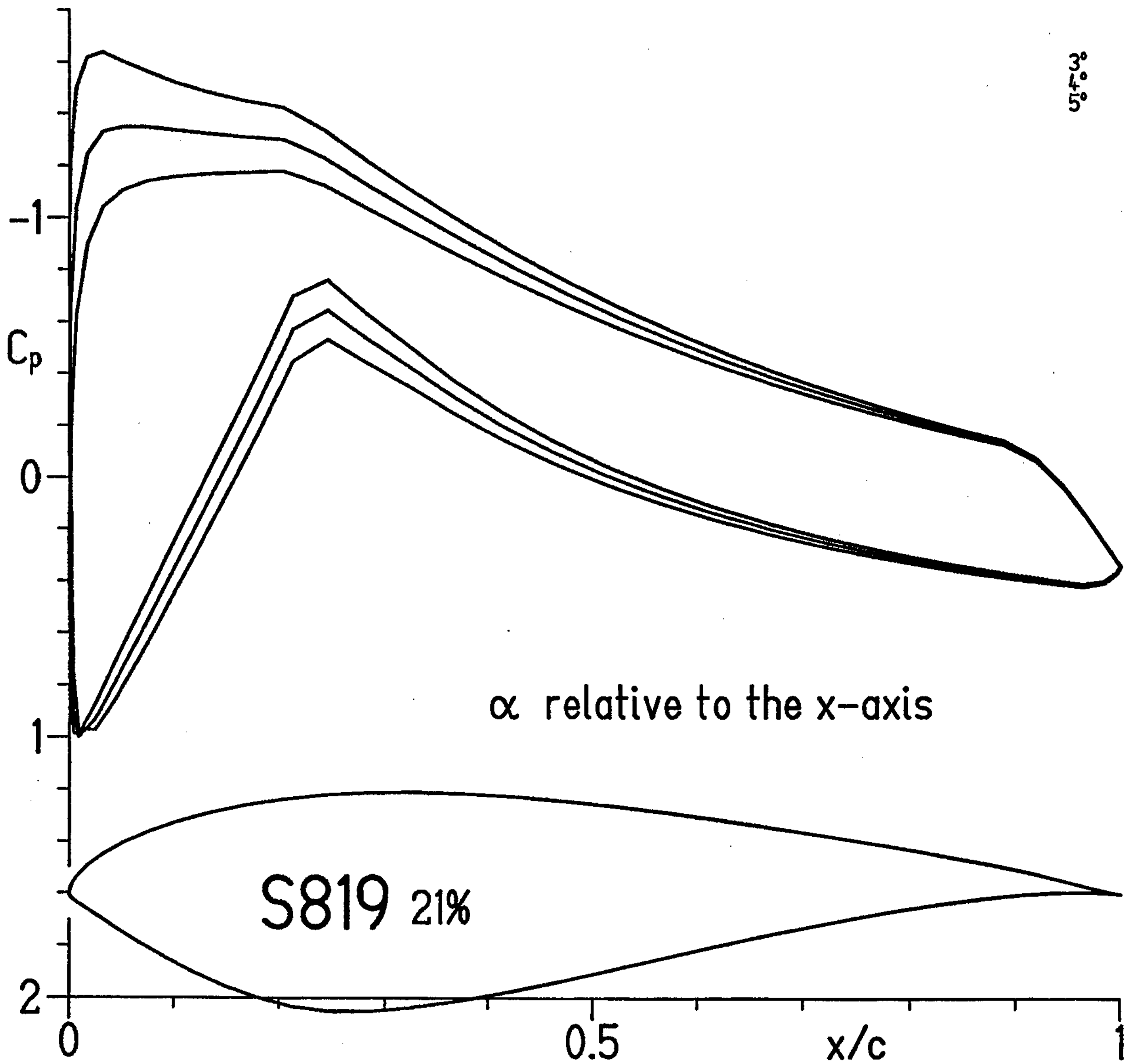

(c) α = 3°, 4°, and 5°.

Figure 2.- Continued.

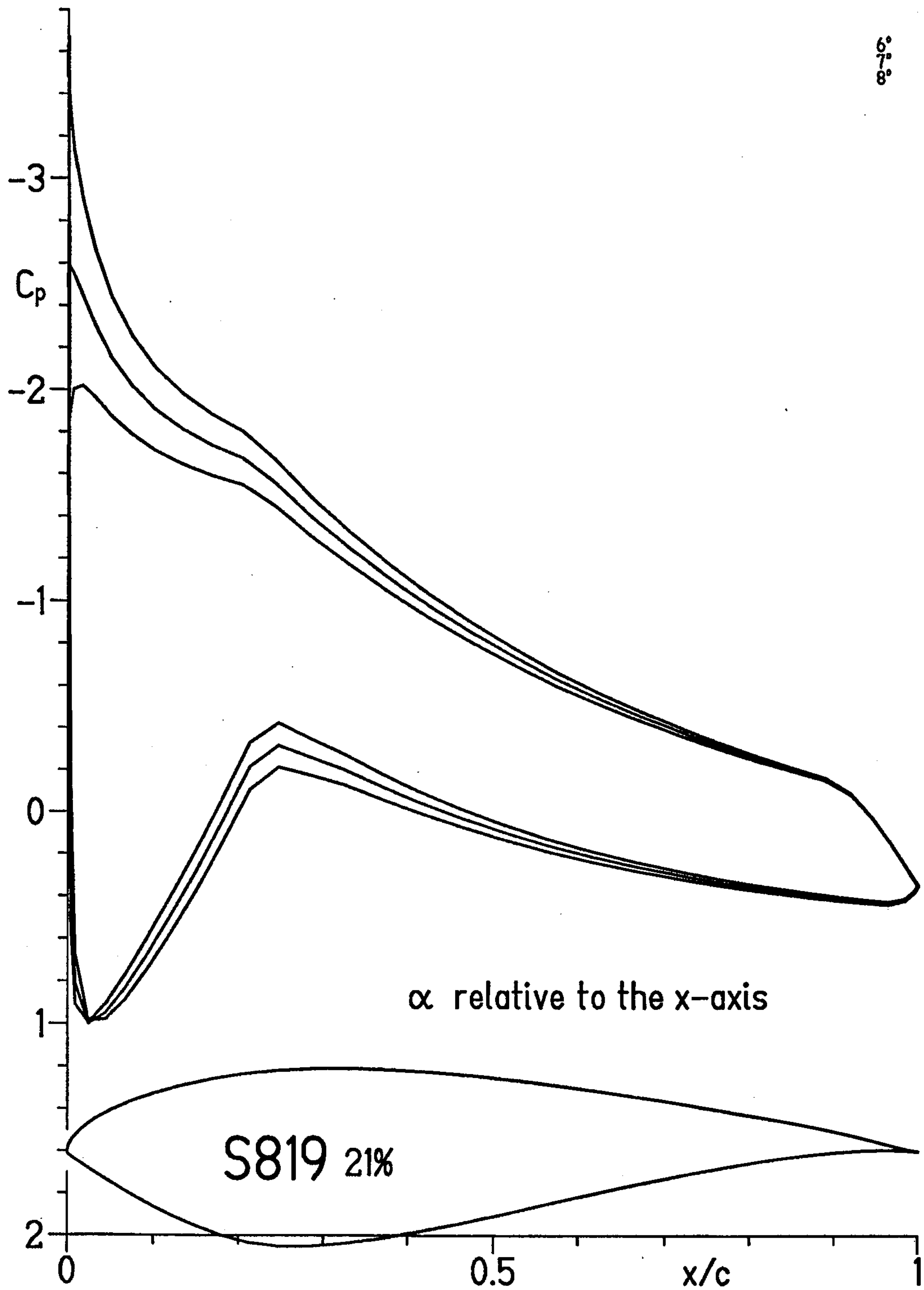

(d) α = 6°, 7°, and 8°.

Figure 2.- Continued.

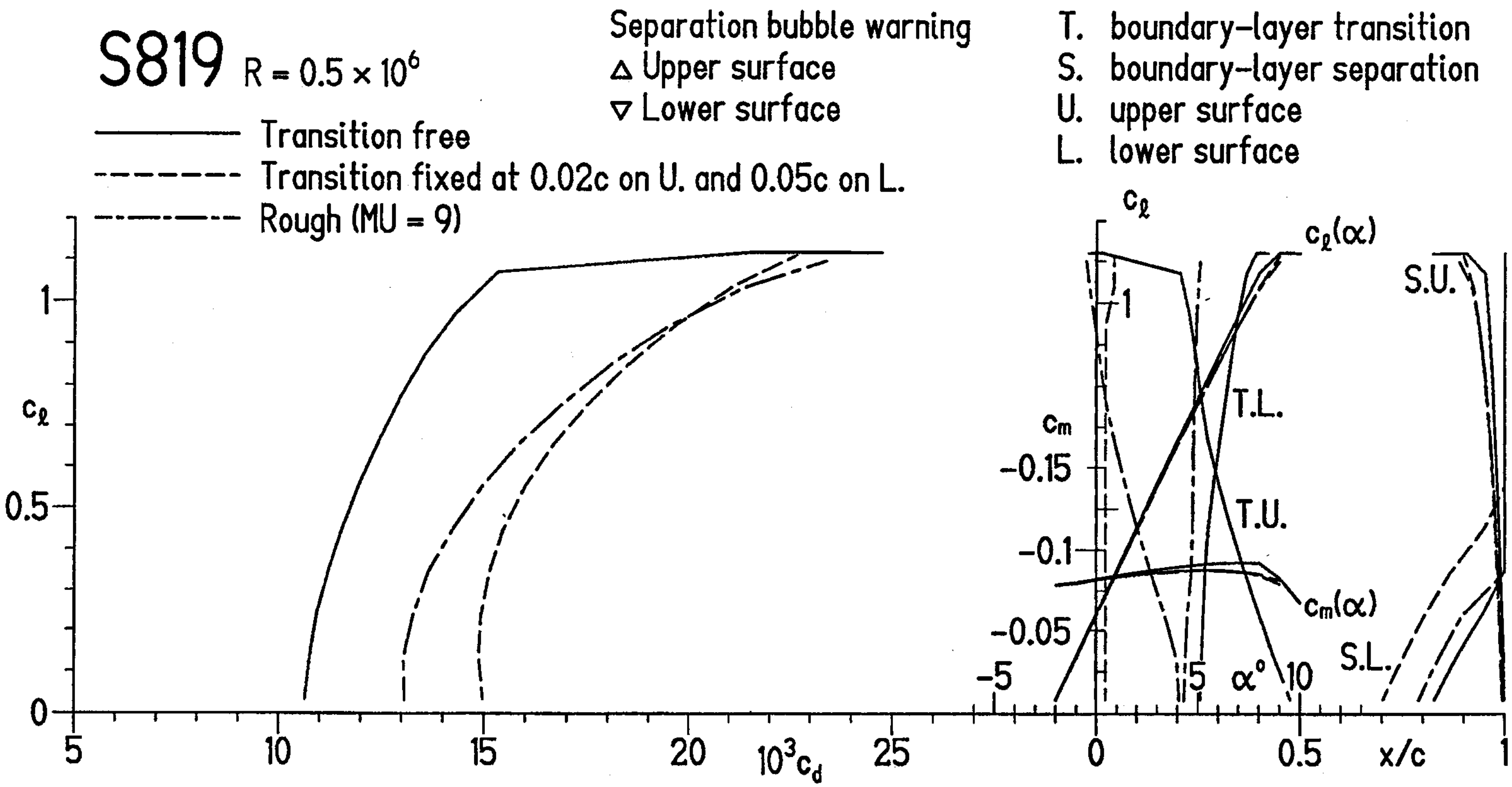

(a) $R = 0.5 \times 10^6$.

Figure 3.- Section characteristics of S819 airfoil with transition free, transition fixed, and rough.

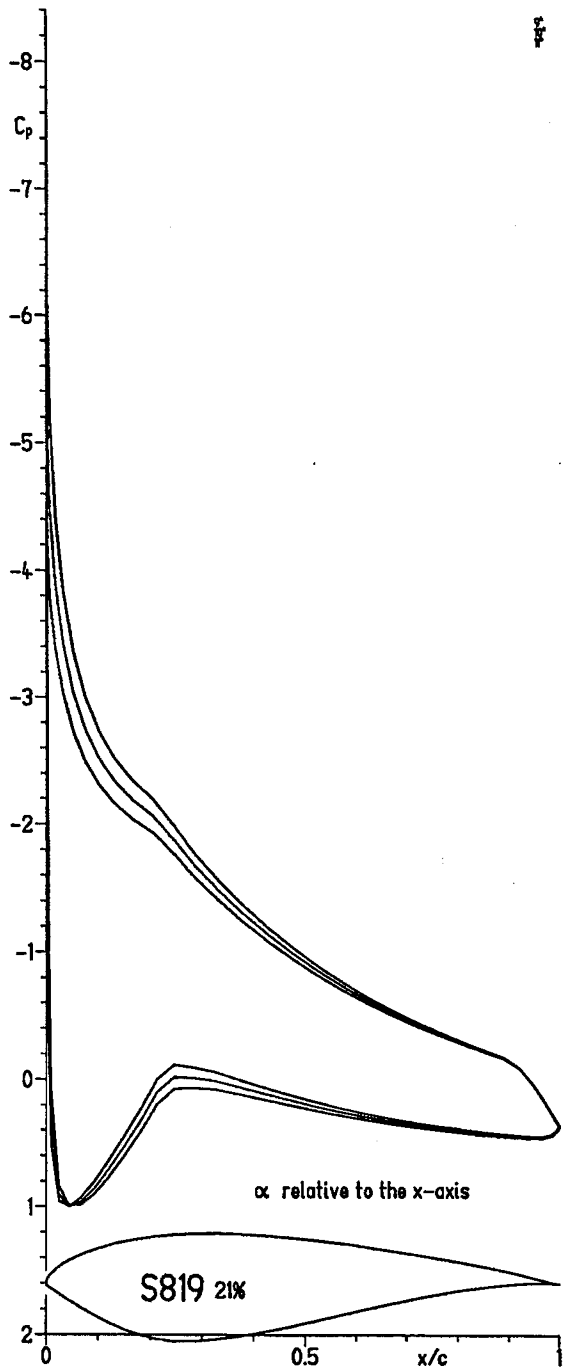

(e) α = 9°, 10°, and 11°.

Figure 2.- Concluded.

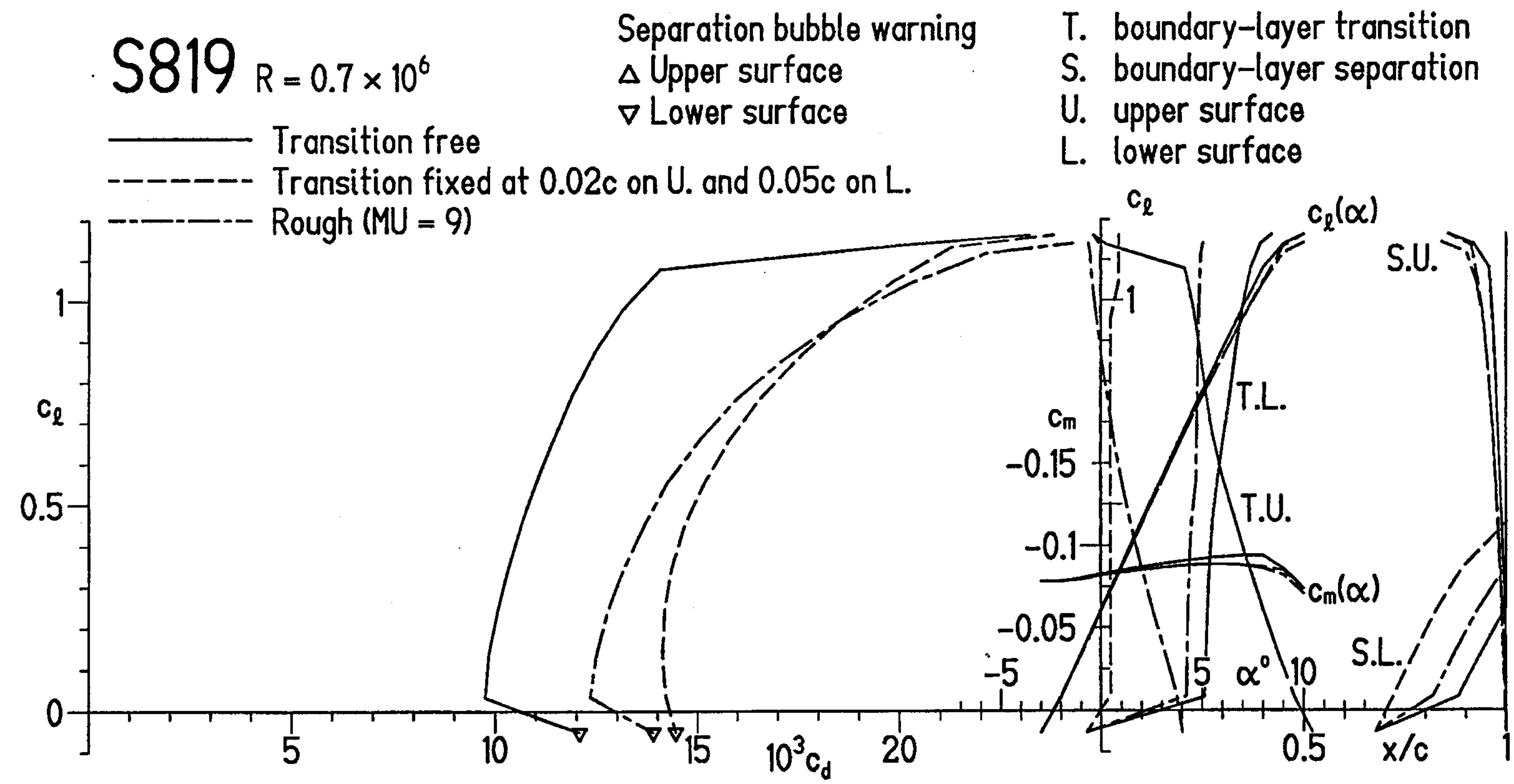

(b) $R = 0.7 \times 10^6$.

Figure 3.- Continued.

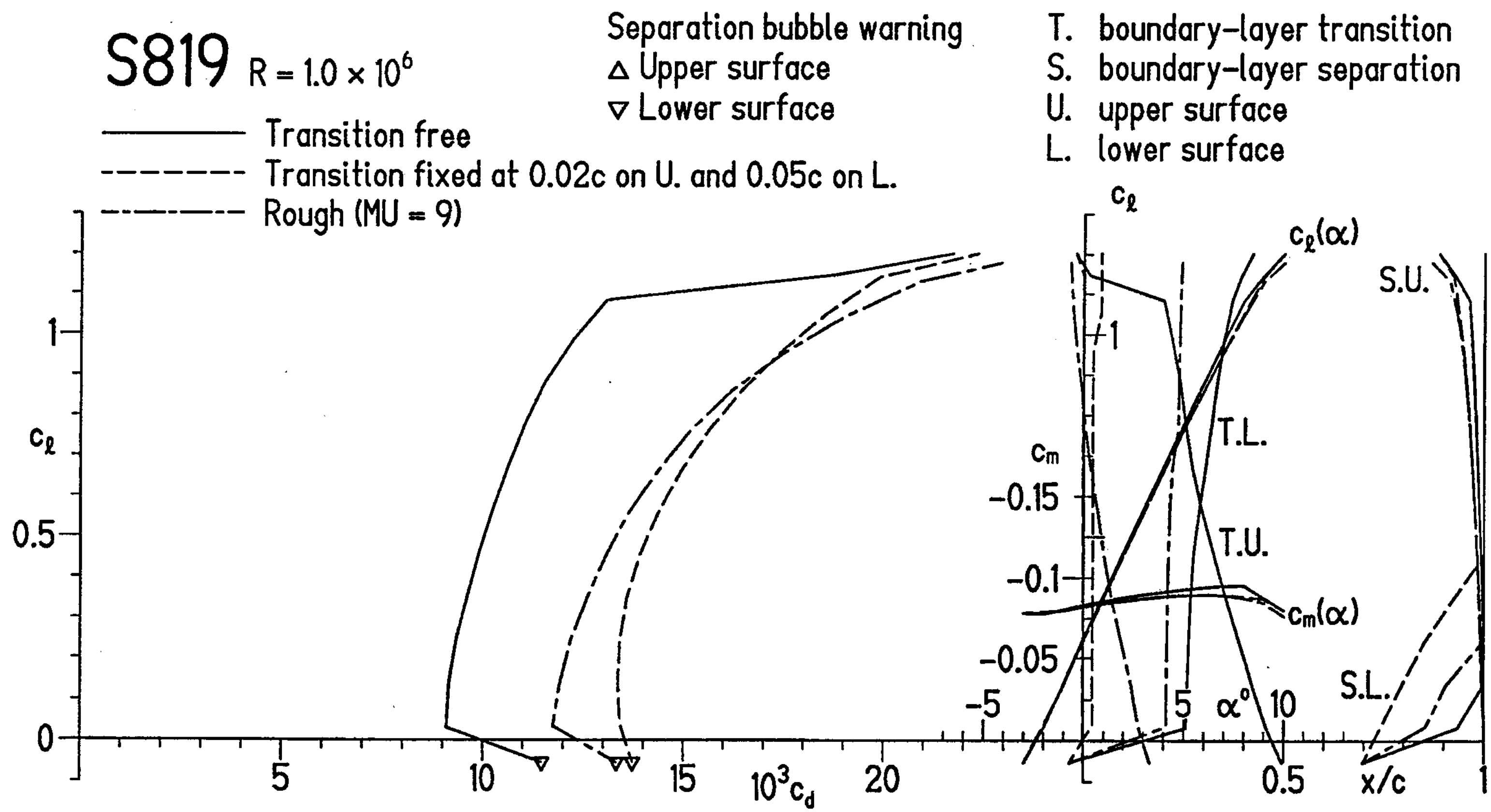

(c) $R = 1.0 \times 10^6$.

Figure 3.- Continued.

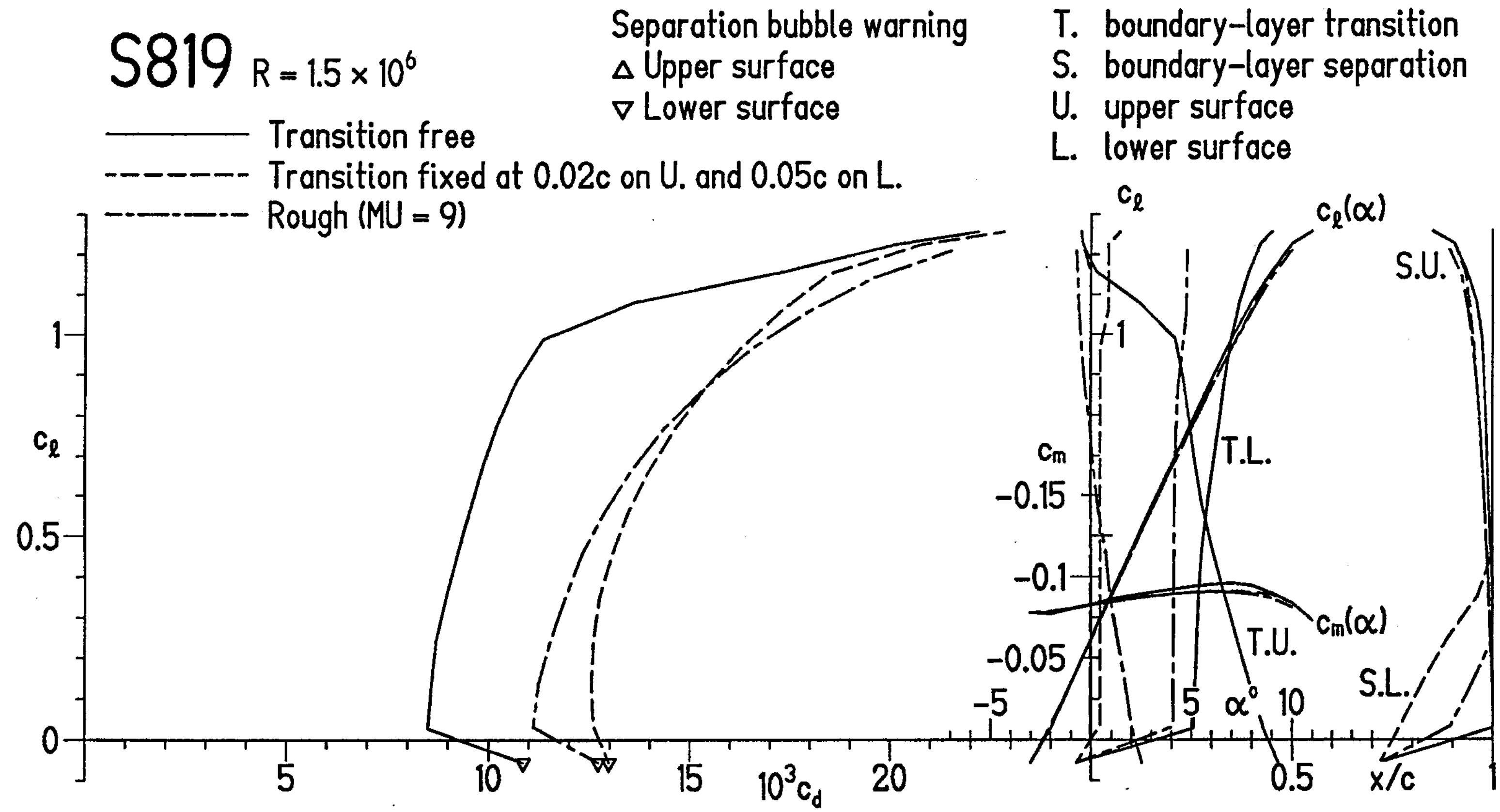

(d) $R = 1.5 \times 10^6$.

Figure 3.- Continued.

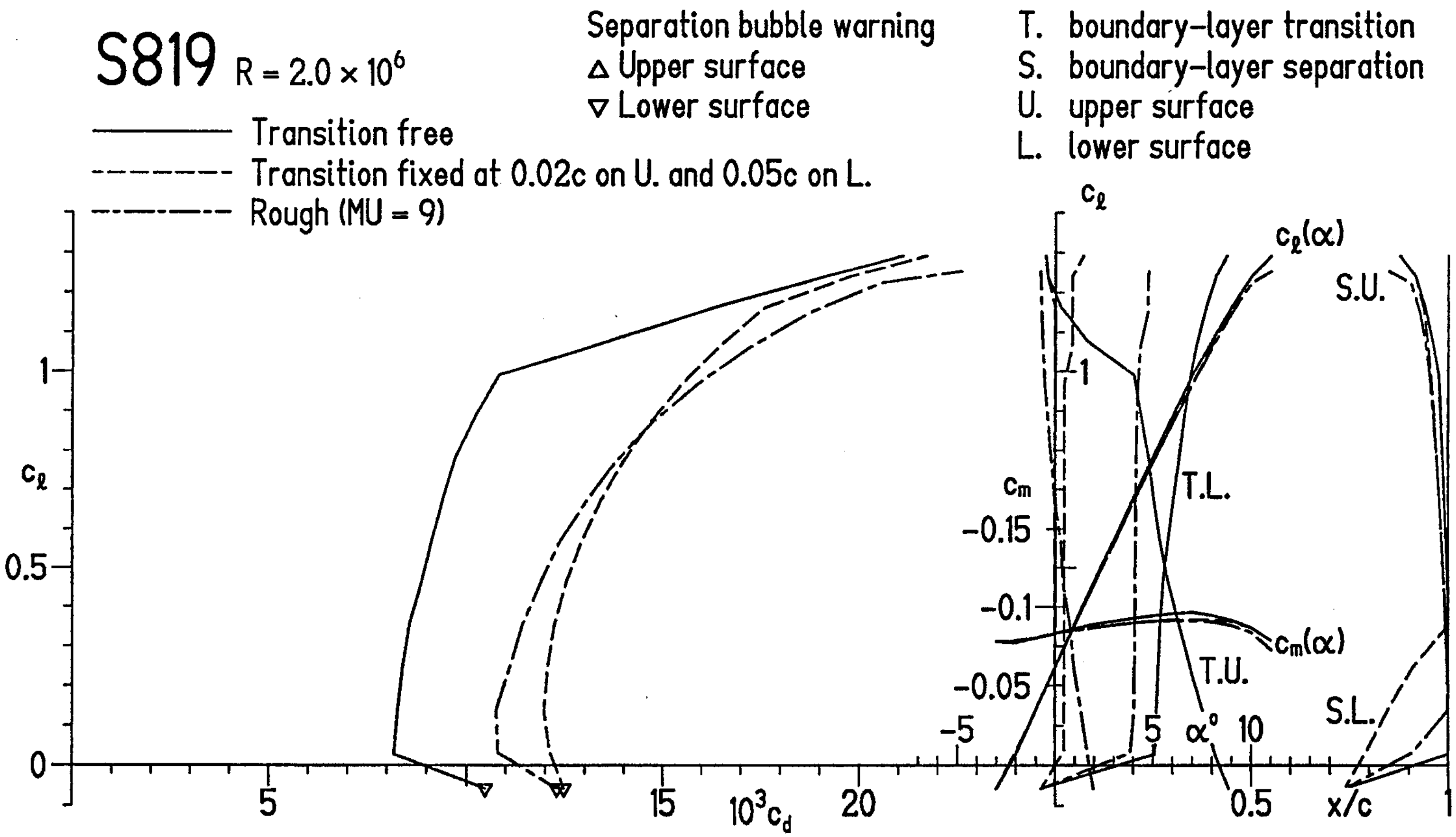

(e) $R = 2.0 \times 10^6$.

Figure 3.- Concluded.

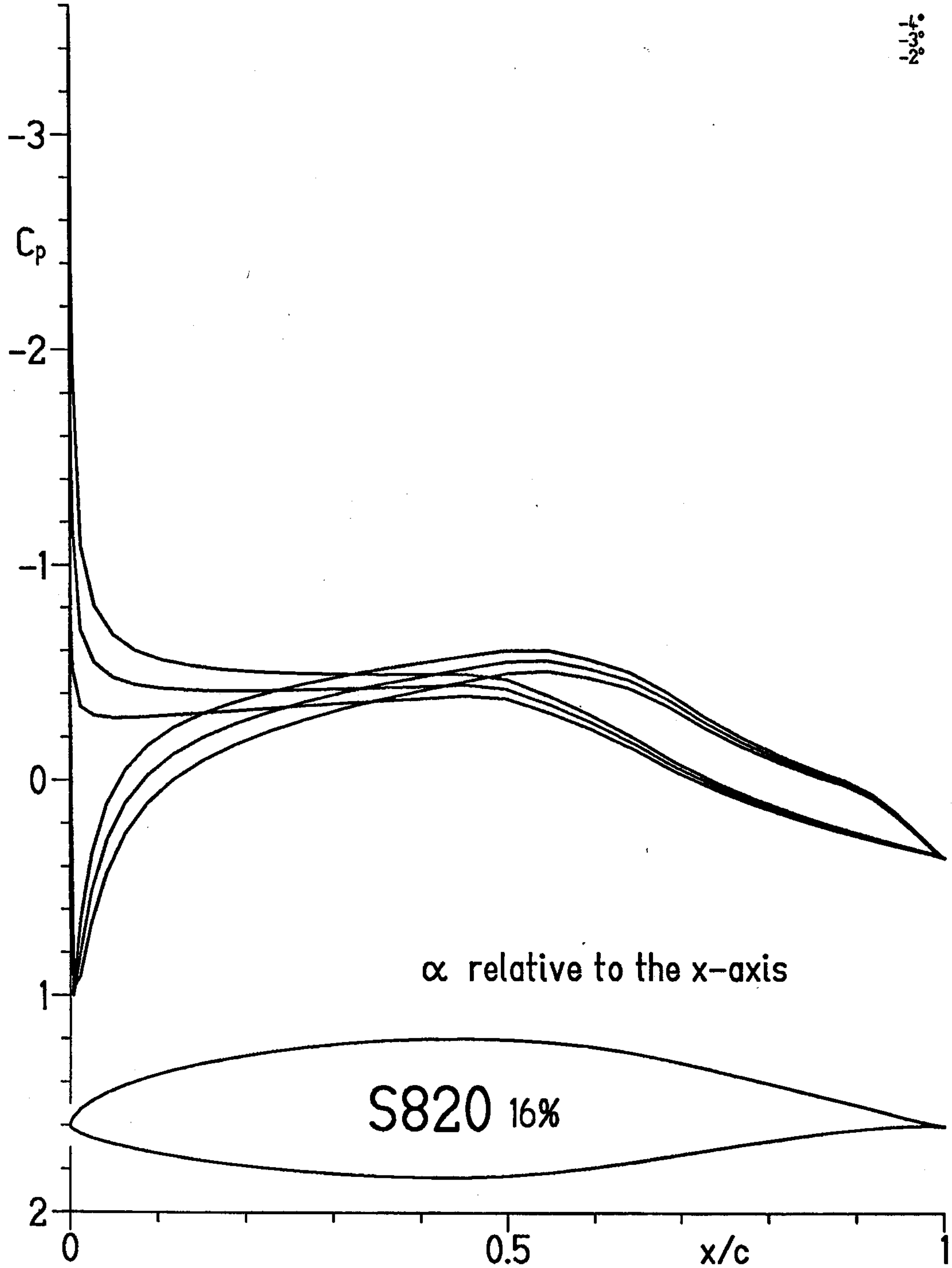

(a) $\alpha = -4°, -3°$, and $-2°$.

Figure 4.- Inviscid pressure distributions for S820 airfoil.

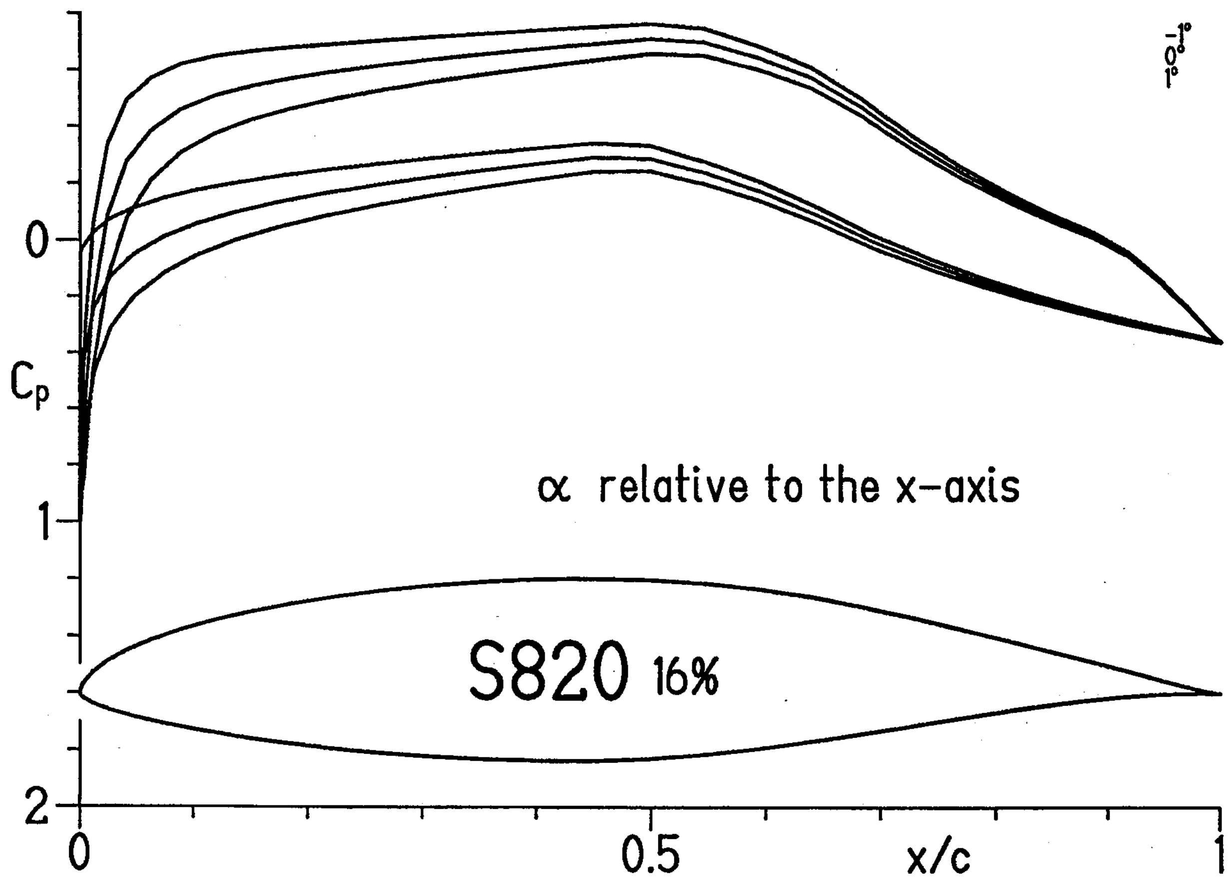

(b) α = −1°, 0°, and 1°.

Figure 4.- Continued.

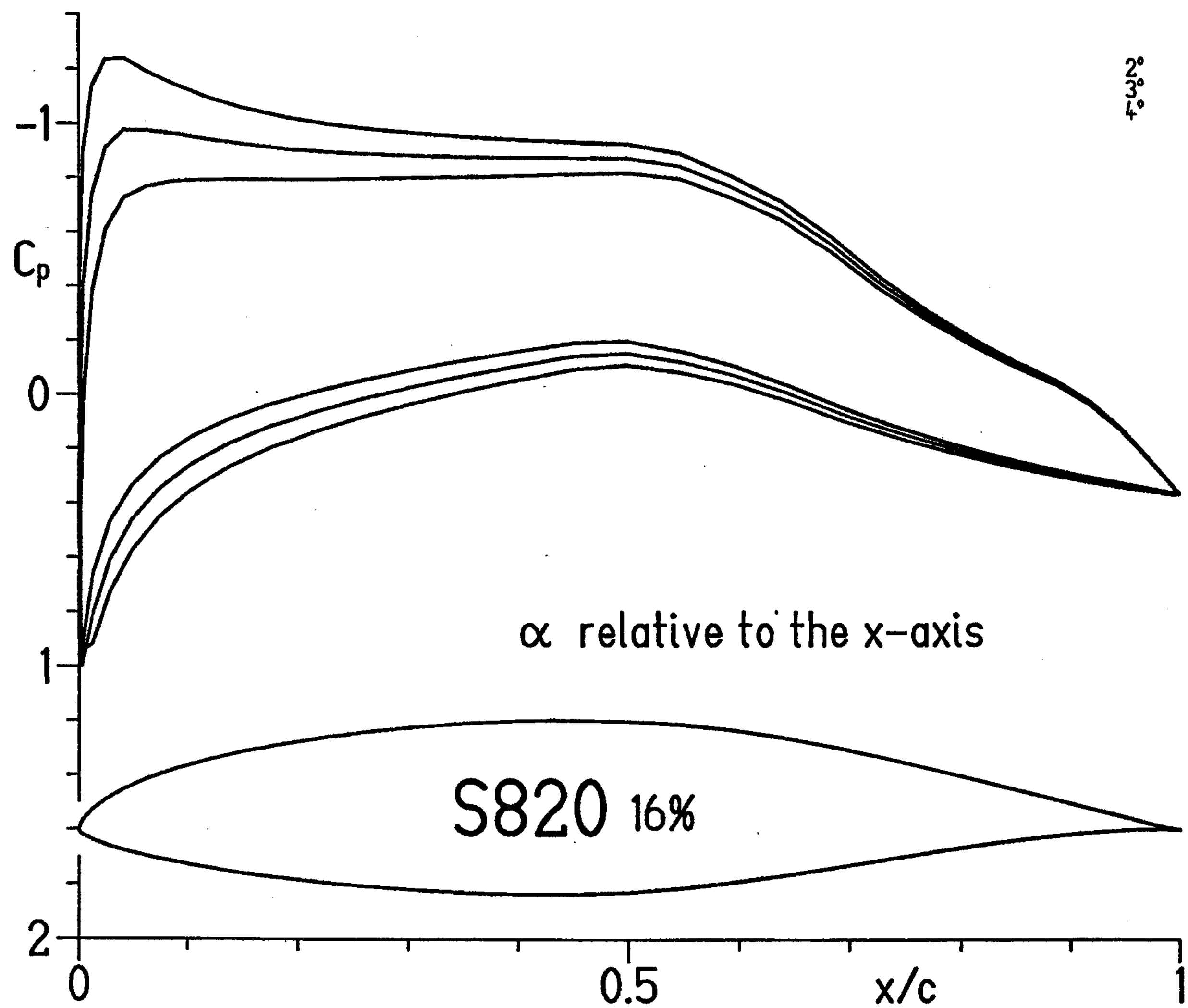

(c) α = 2°, 3°, and 4°.

Figure 4.- Continued.

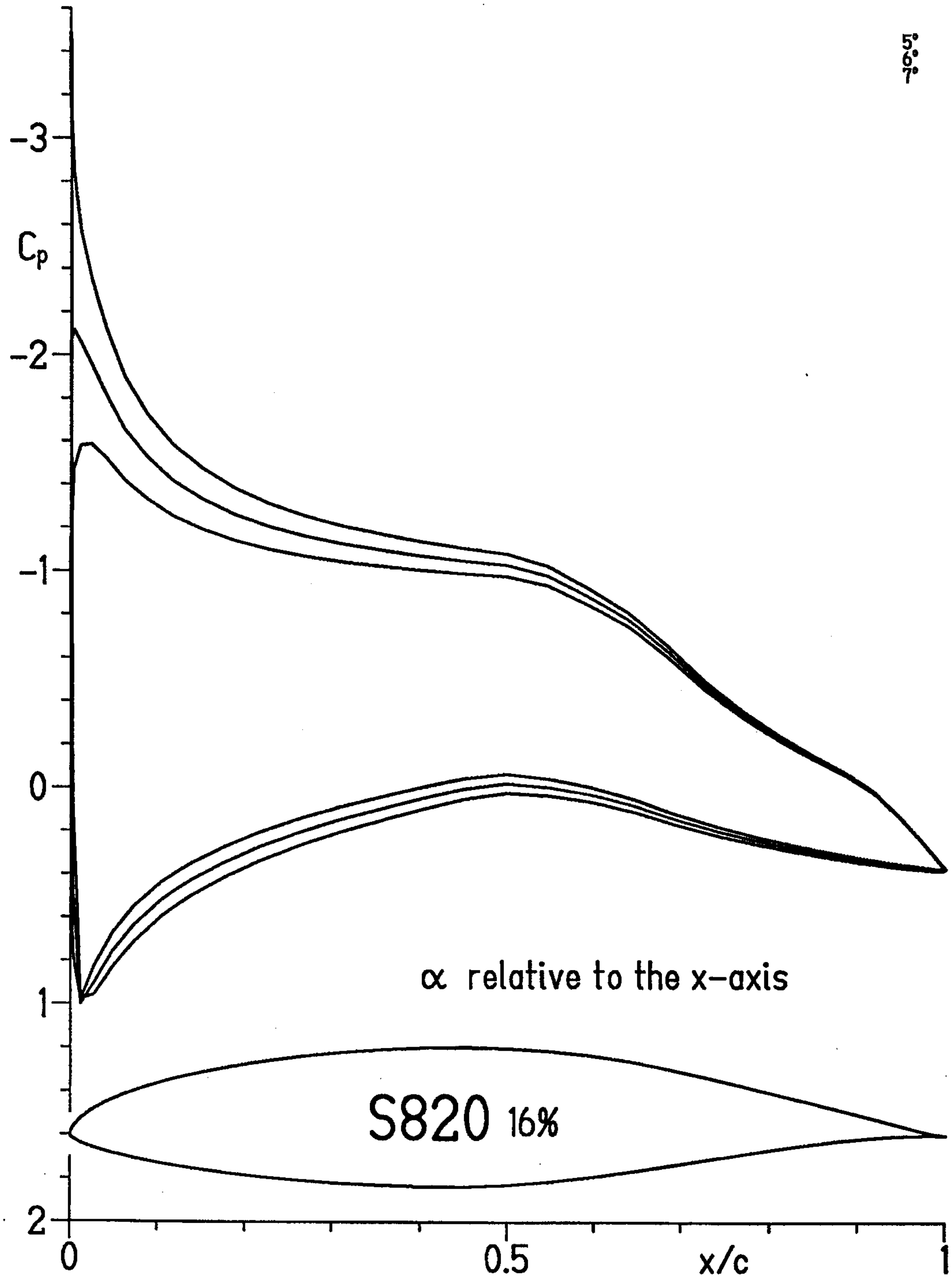

(d) α = 5°, 6°, and 7°.

Figure 4.- Continued.

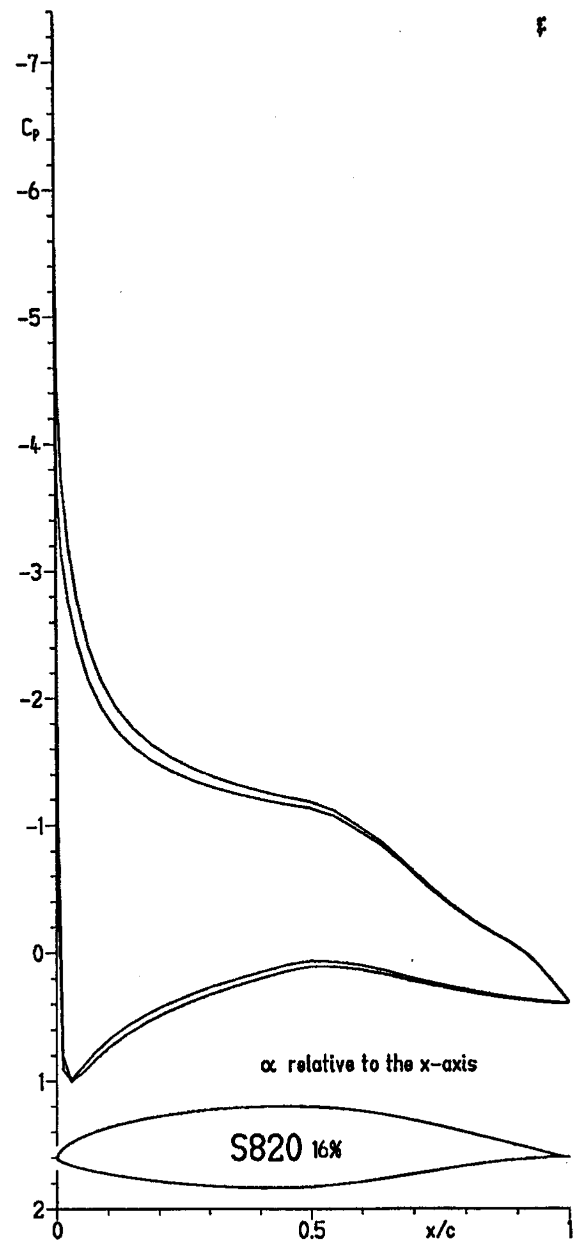

(e) α = 8° and 9°.

Figure 4.- Concluded.

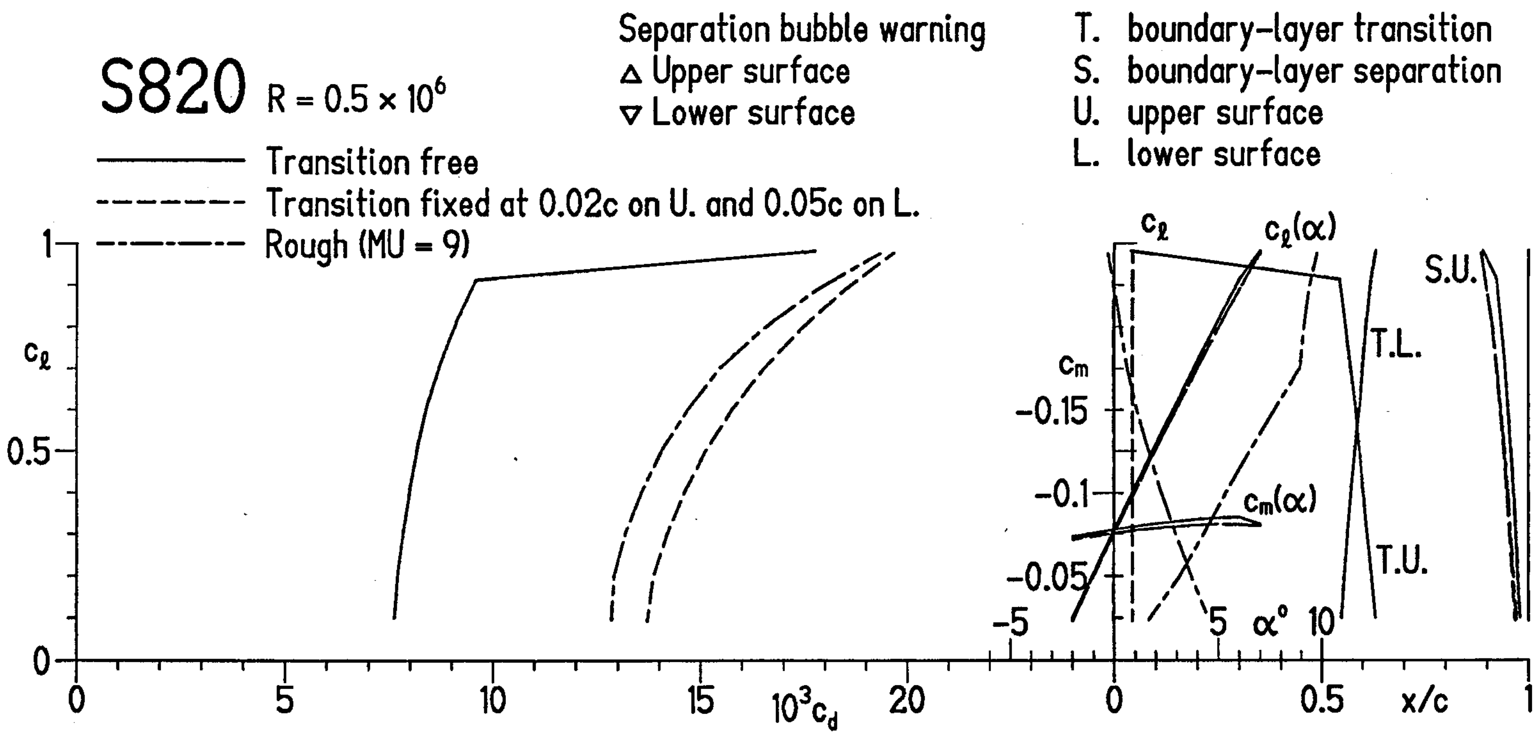

(a) $R = 0.5 \times 10^6$.

Figure 5.- Section characteristics of S820 airfoil with transition free, transition fixed, and rough.

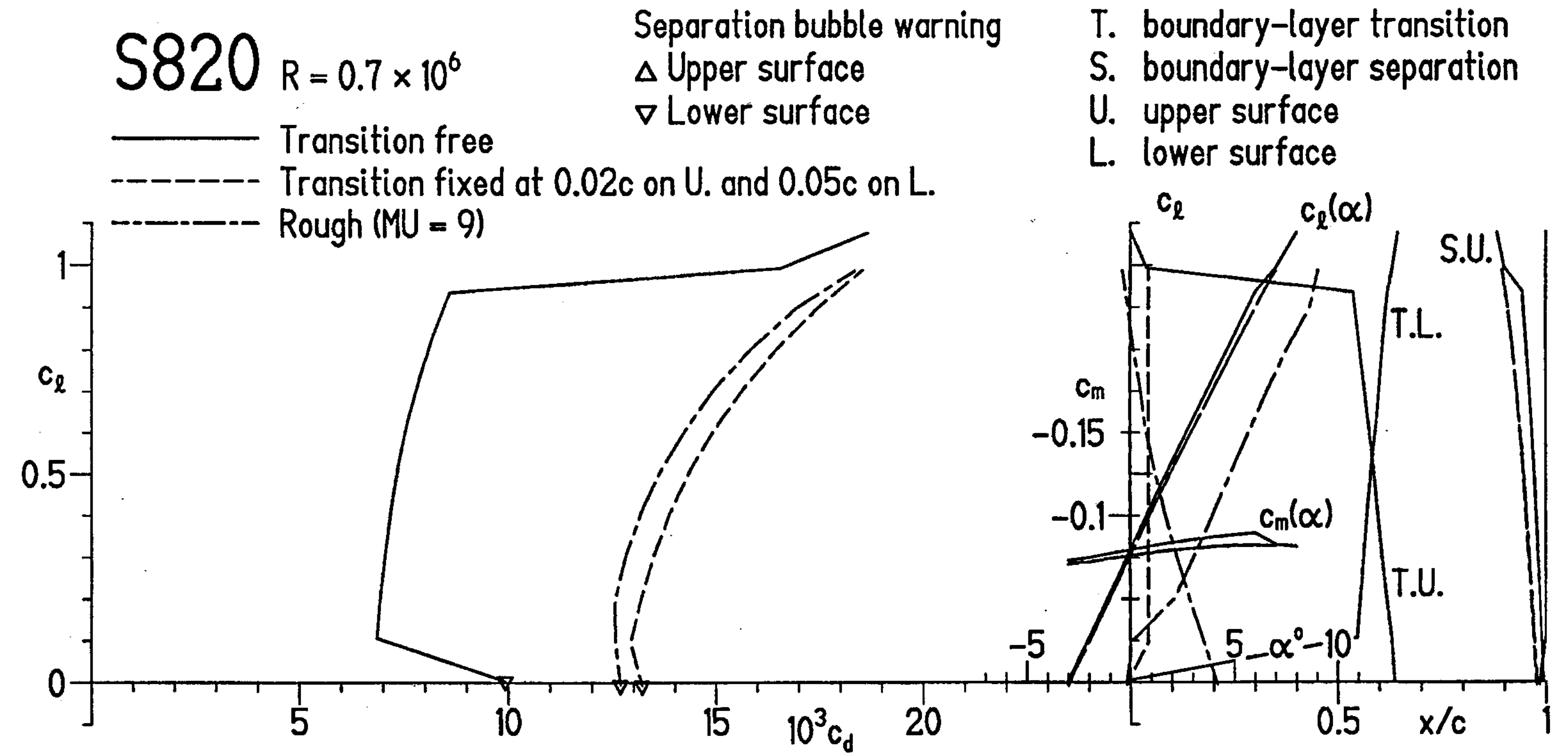

(b) $R = 0.7 \times 10^6$.

Figure 5.- Continued.

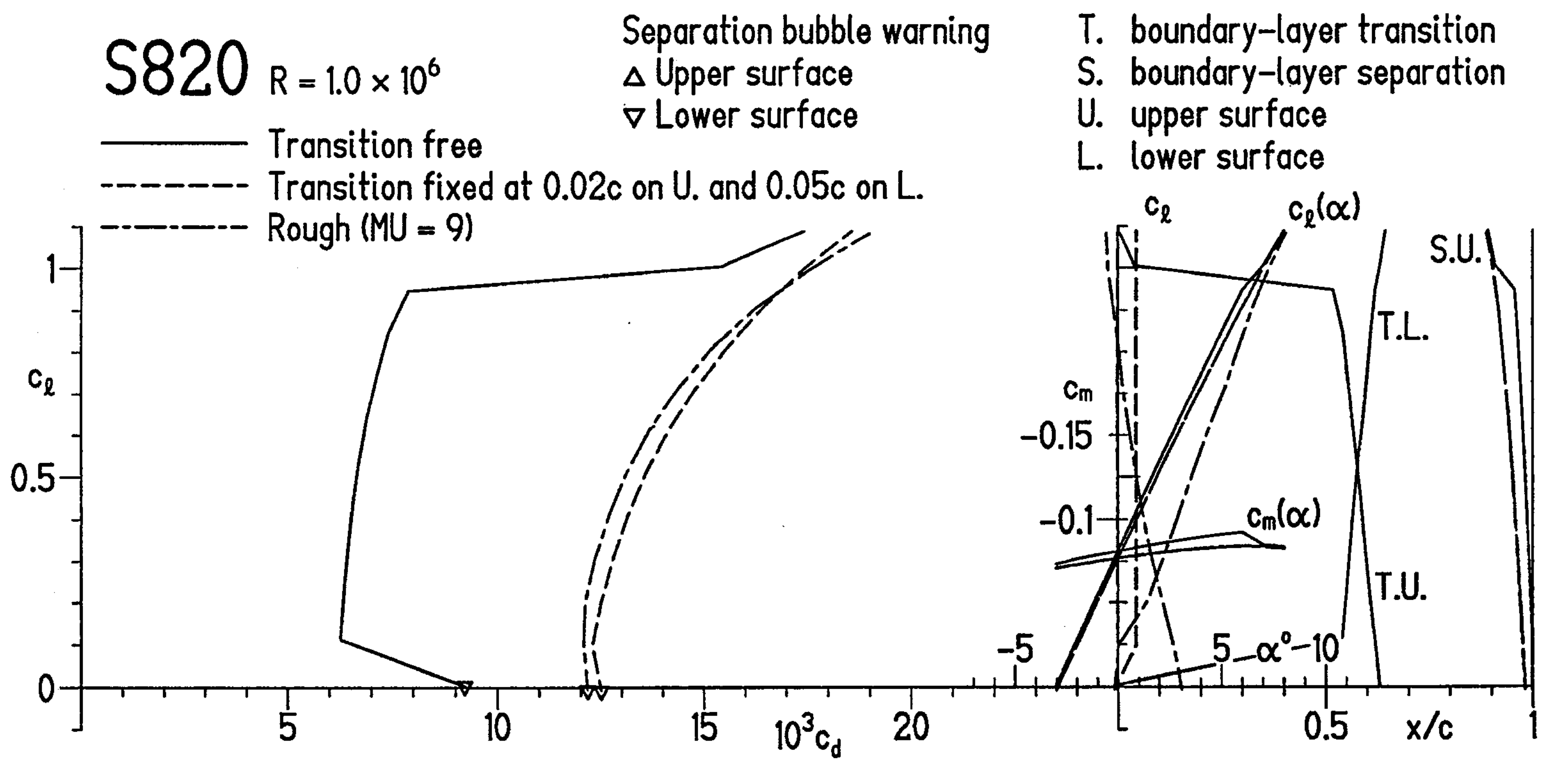

(c) $R = 1.0 \times 10^6$.

Figure 5.- Continued.

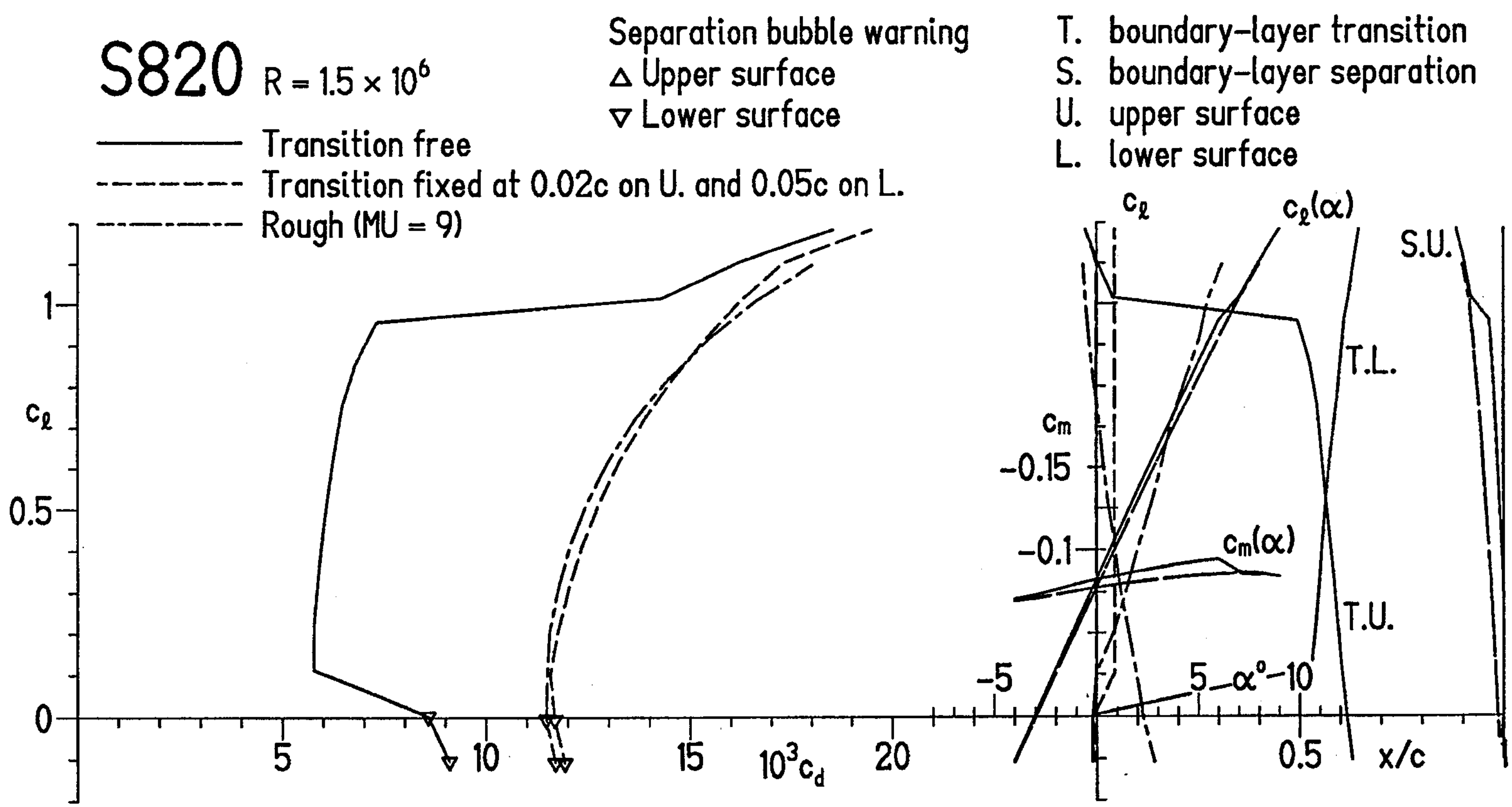

(d) $R = 1.5 \times 10^6$.

Figure 5.- Continued.

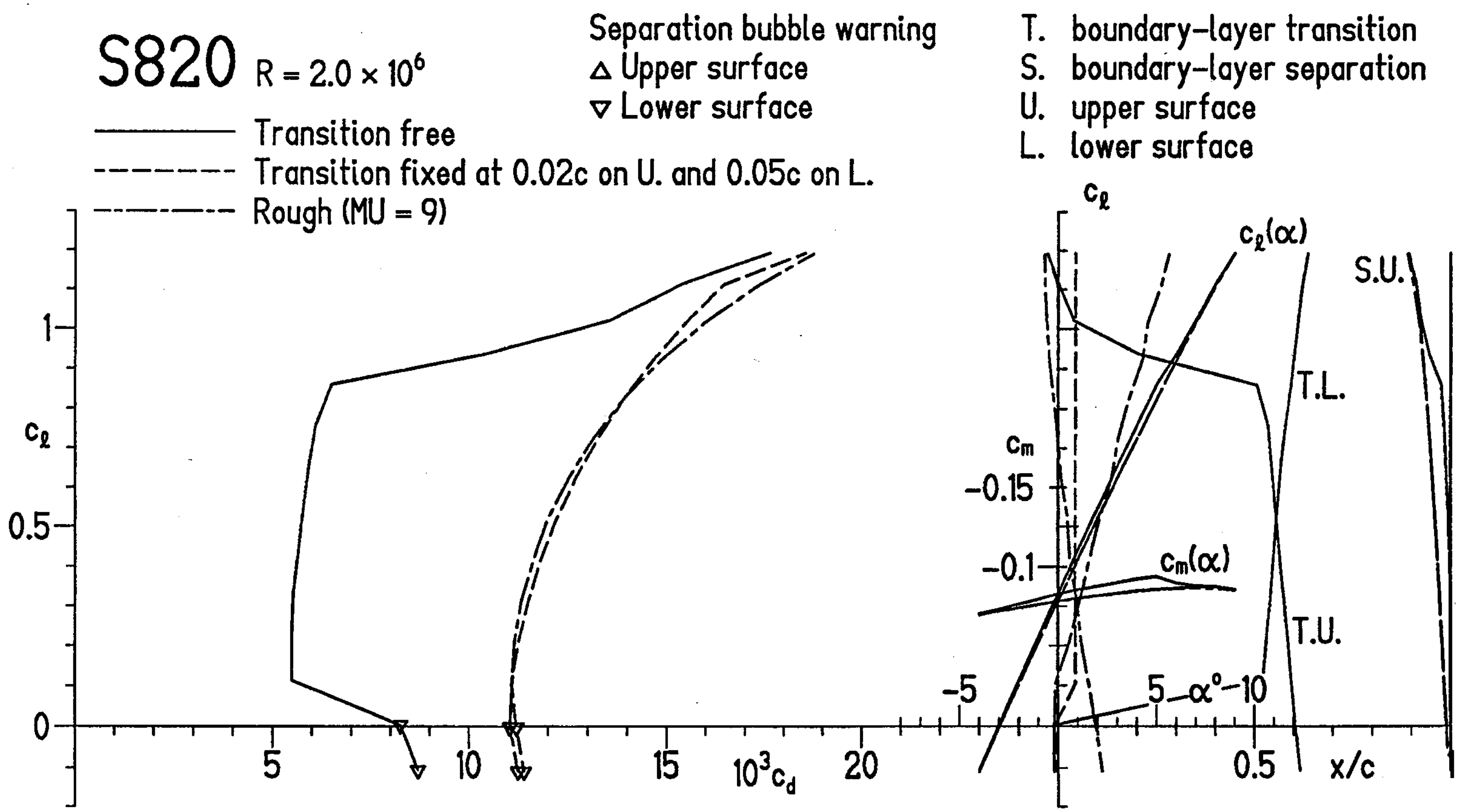

(e) $R = 2.0 \times 10^6$.

Figure 5.- Concluded.

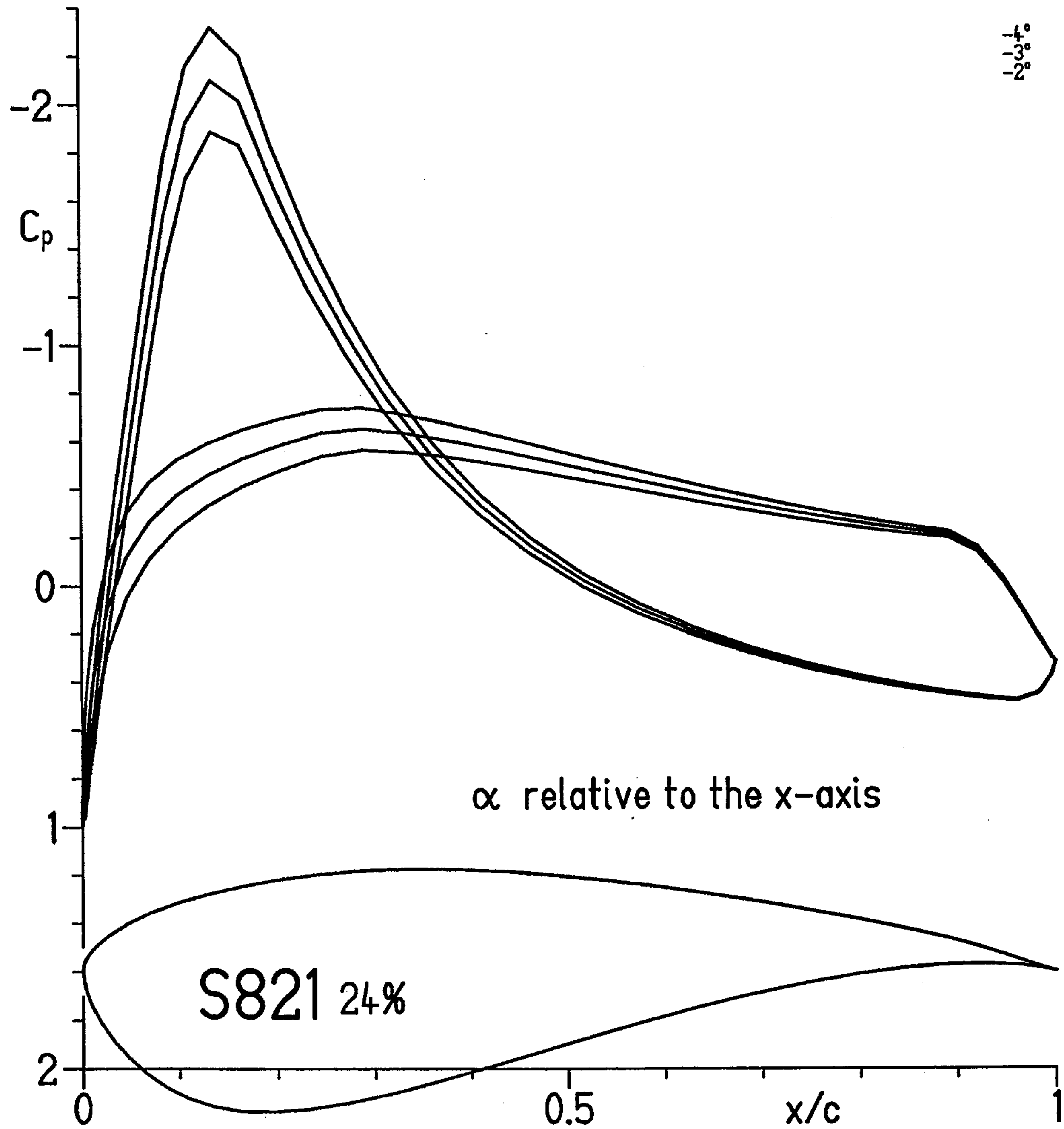

(a) α = –4°, –3°, and –2°.

Figure 6.- Inviscid pressure distributions for S821 airfoil.

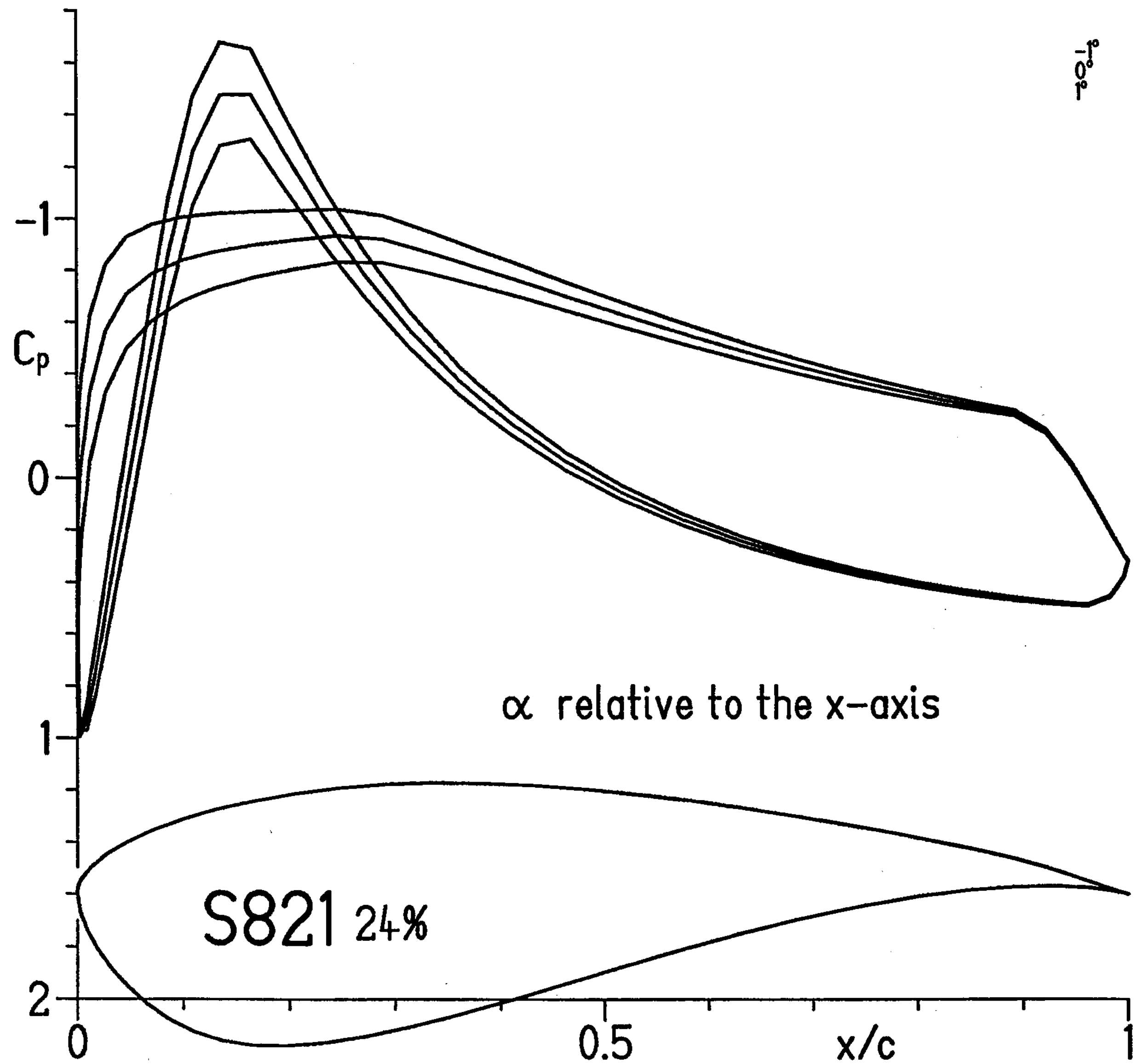

(b) α = −1°, 0°, and 1°.

Figure 6.- Continued.

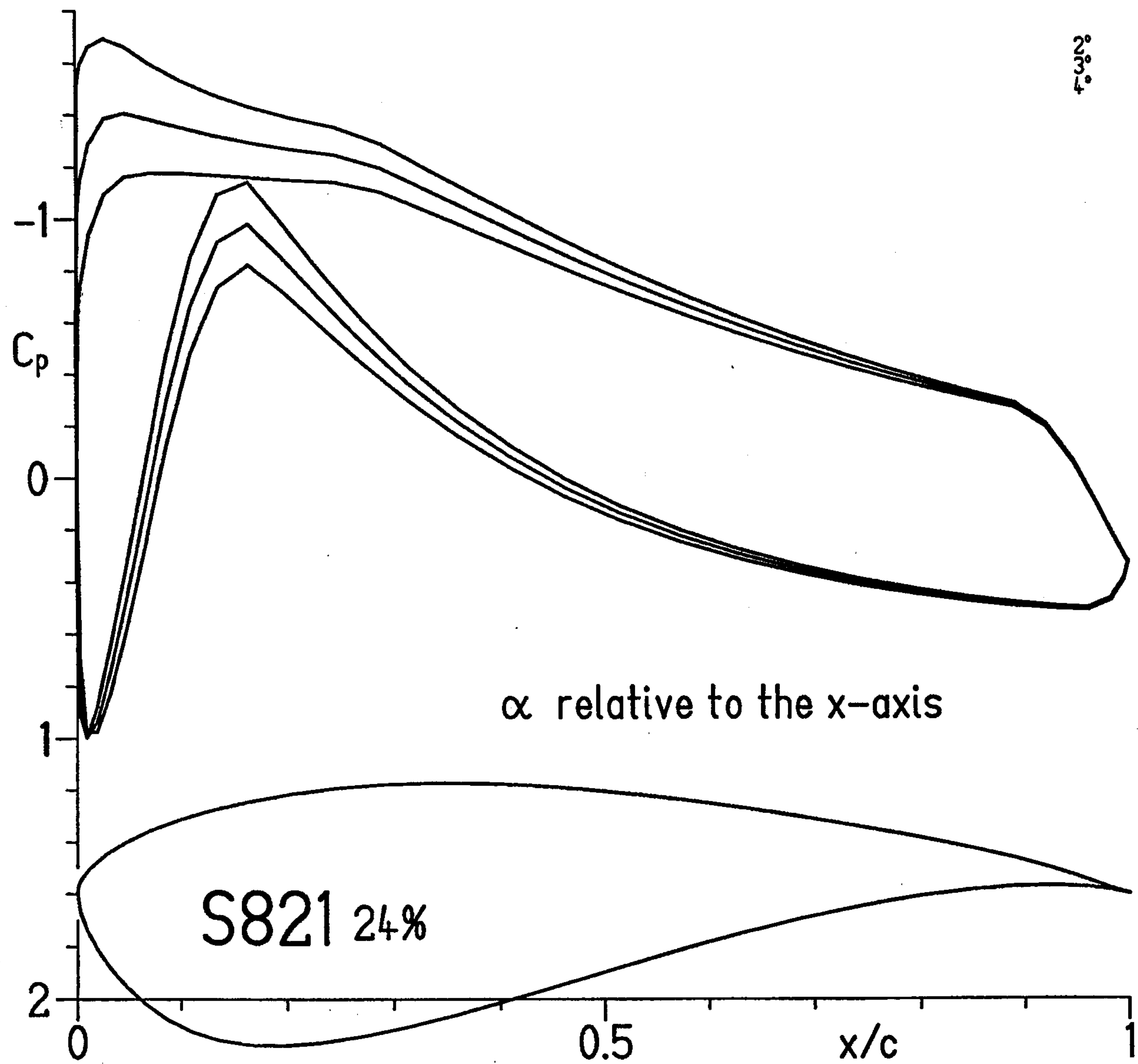

(c) α = 2°, 3°, and 4°.

Figure 6.- Continued.

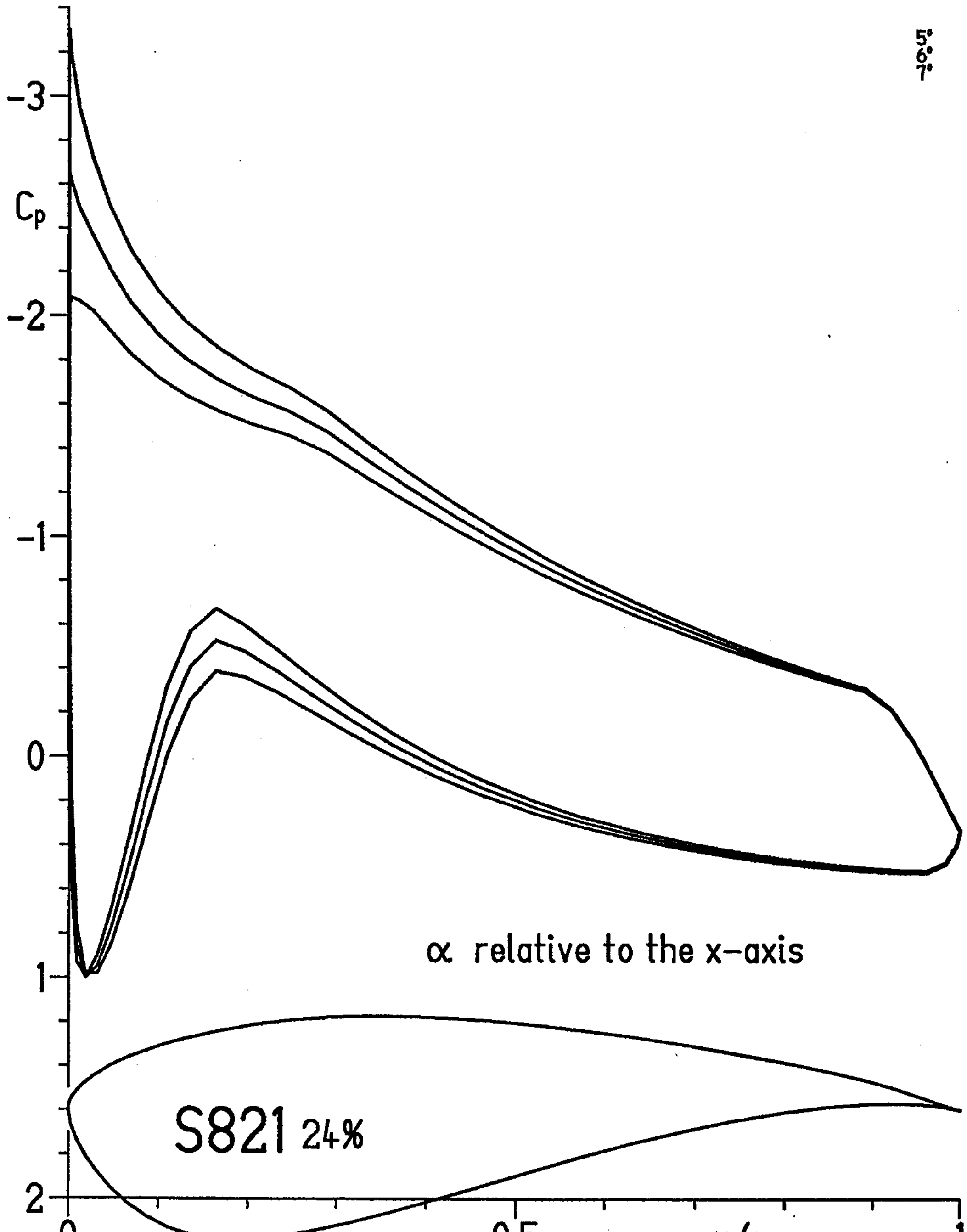

(d) $\alpha = 5°, 6°$, and $7°$.

Figure 6.- Continued.

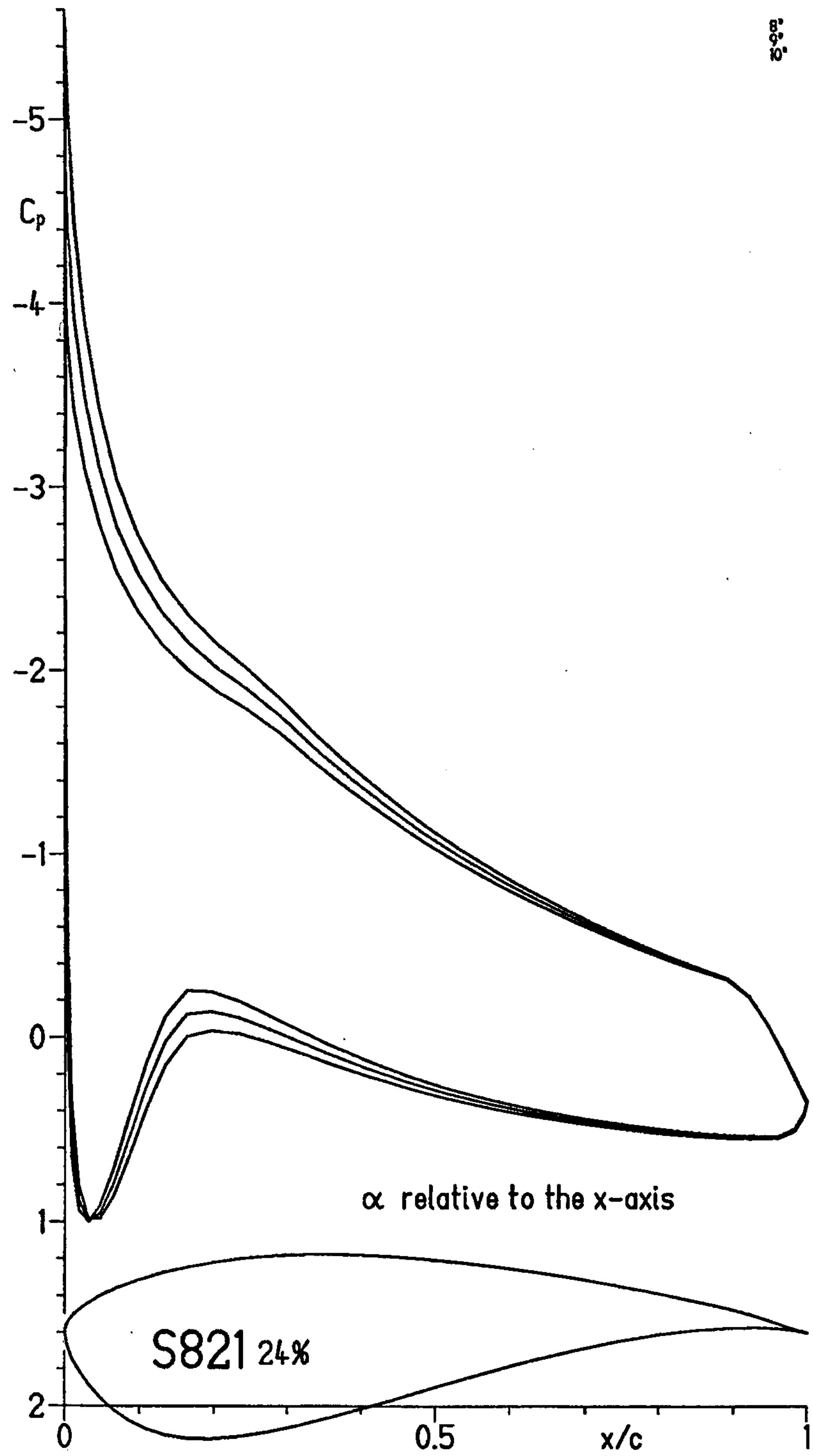

(e) $\alpha = 8°, 9°$, and $10°$.

Figure 6.- Continued.

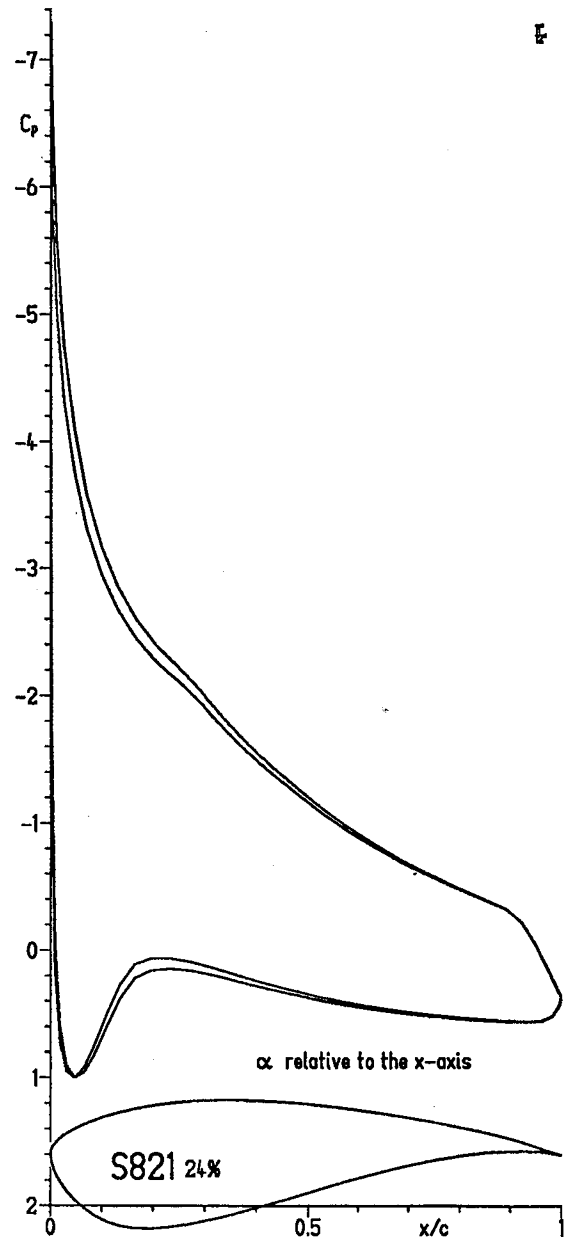

(f) $\alpha = 11°$ and $12°$.

Figure 6.- Concluded.

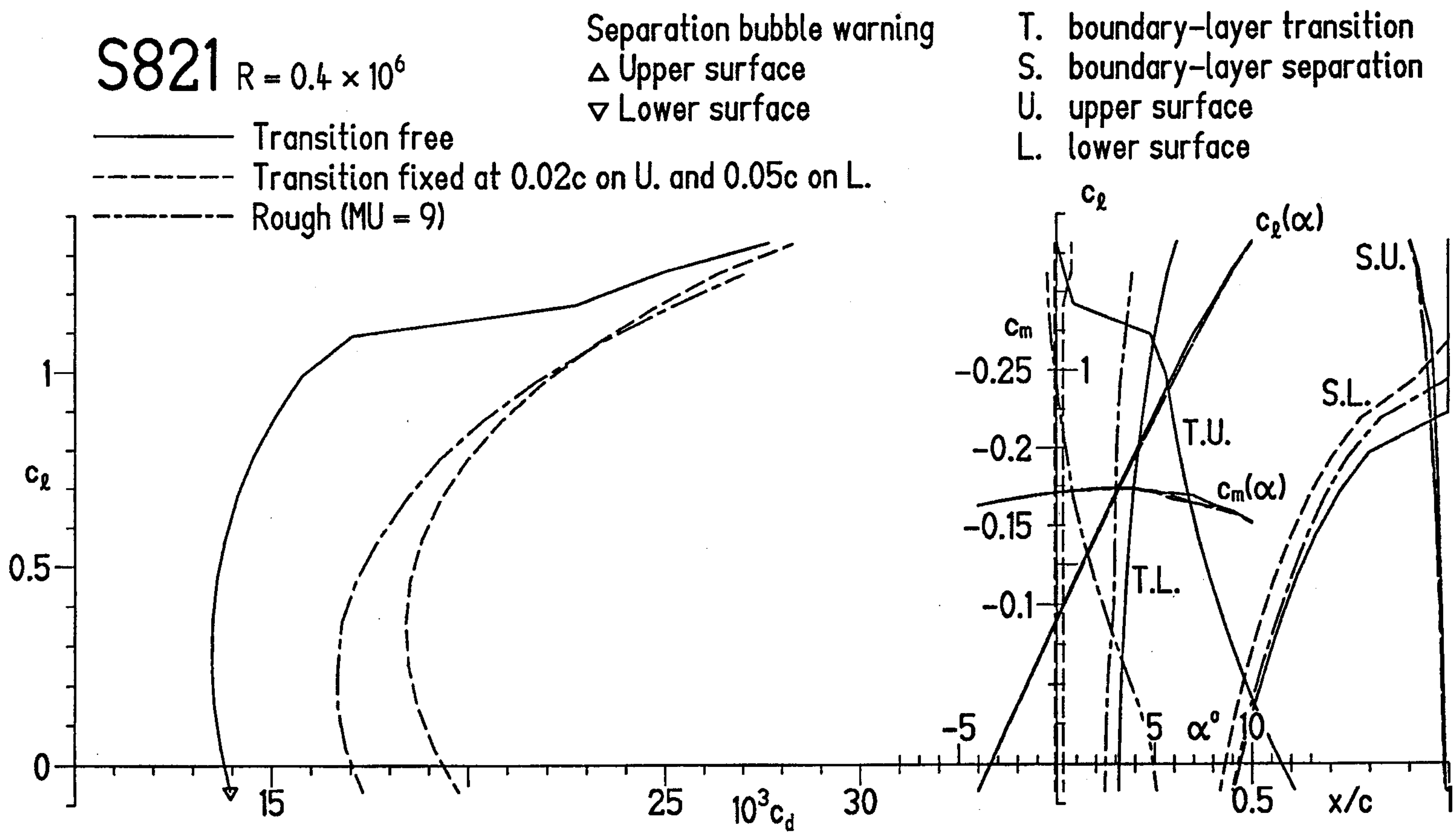

(a) $R = 0.4 \times 10^6$.

Figure 7.- Section characteristics of S821 airfoil with transition free, transition fixed, and rough.

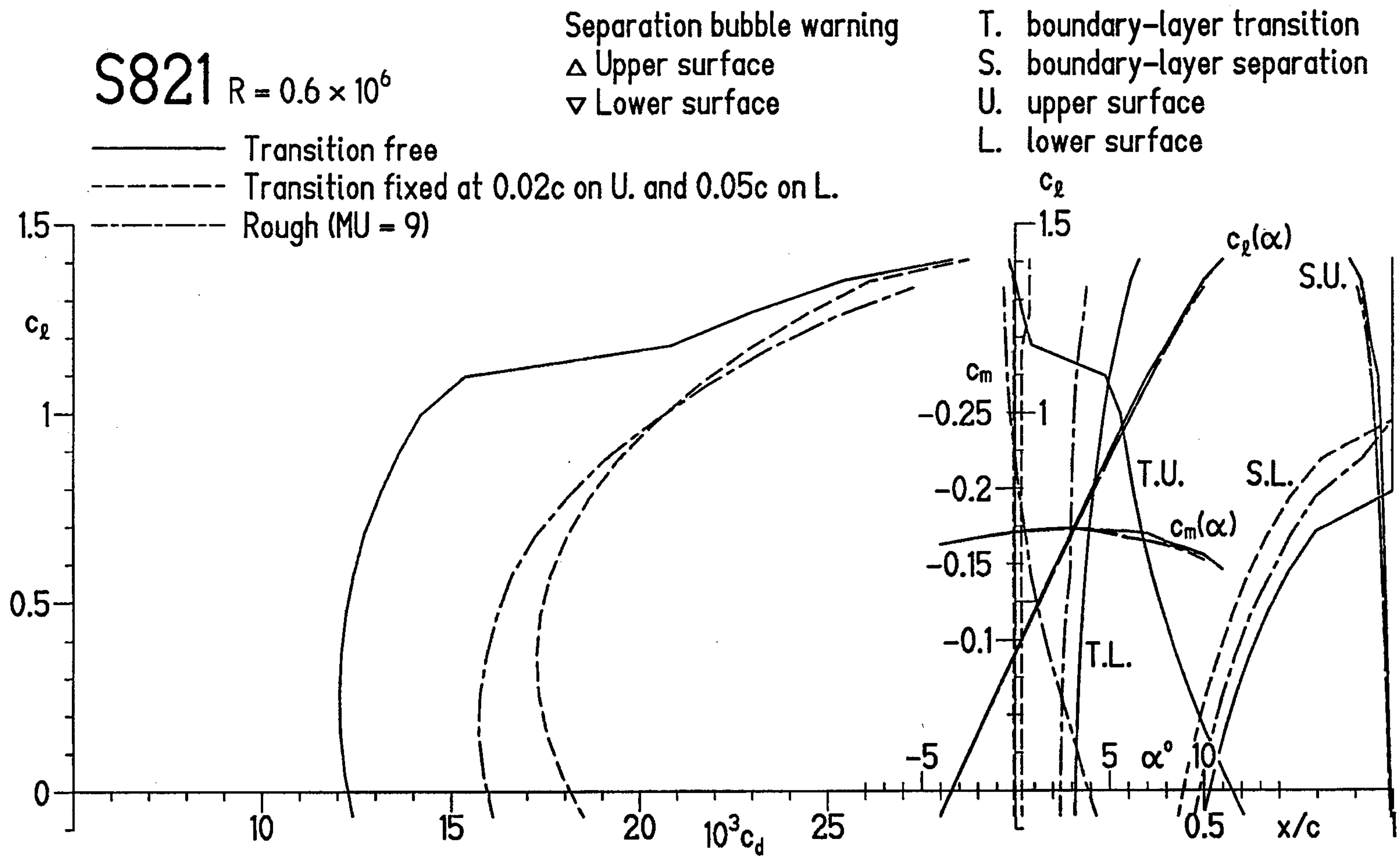

(b) $R = 0.6 \times 10^6$.

Figure 7.- Continued.

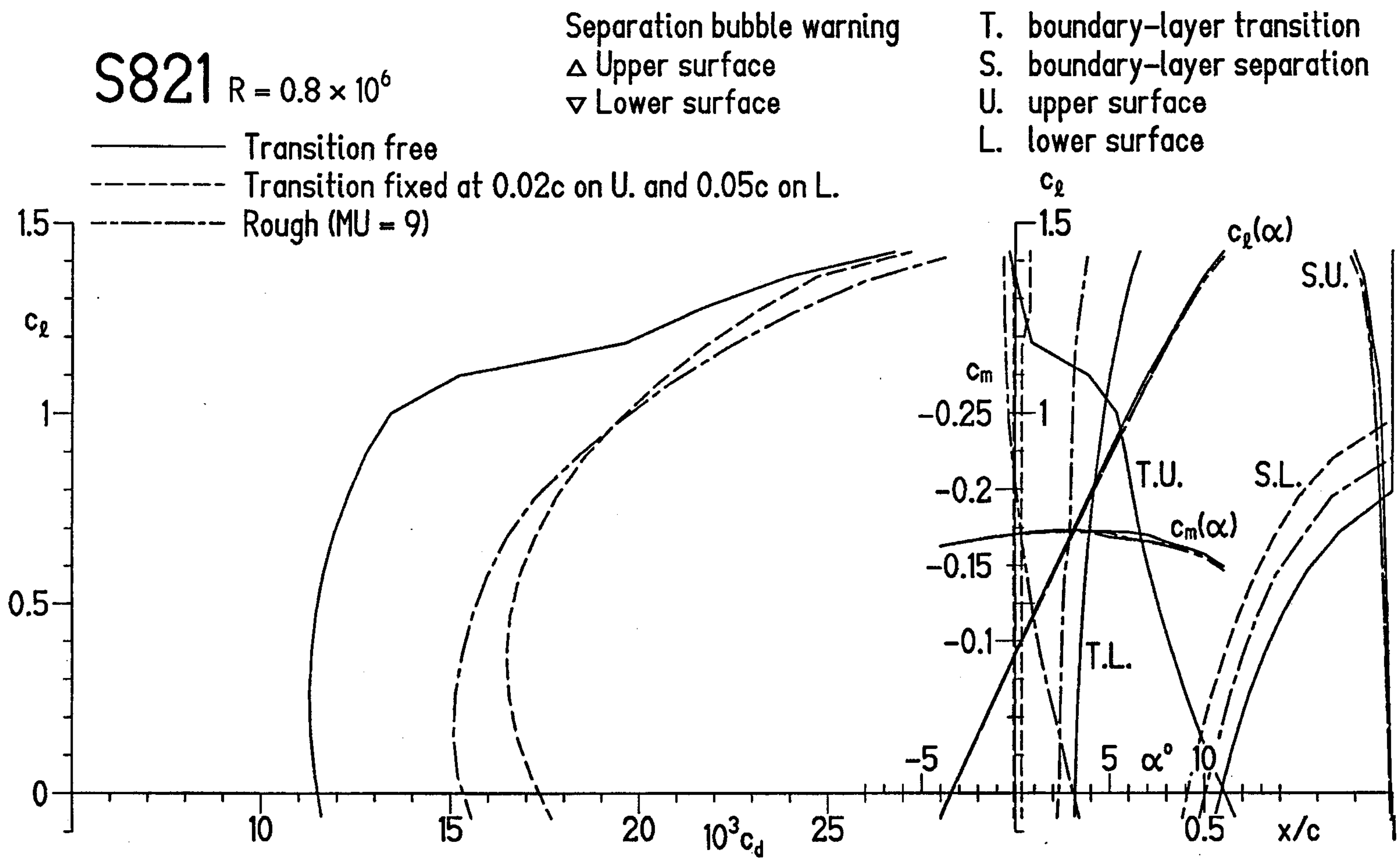

(c) $R = 0.8 \times 10^6$.

Figure 7.- Continued.

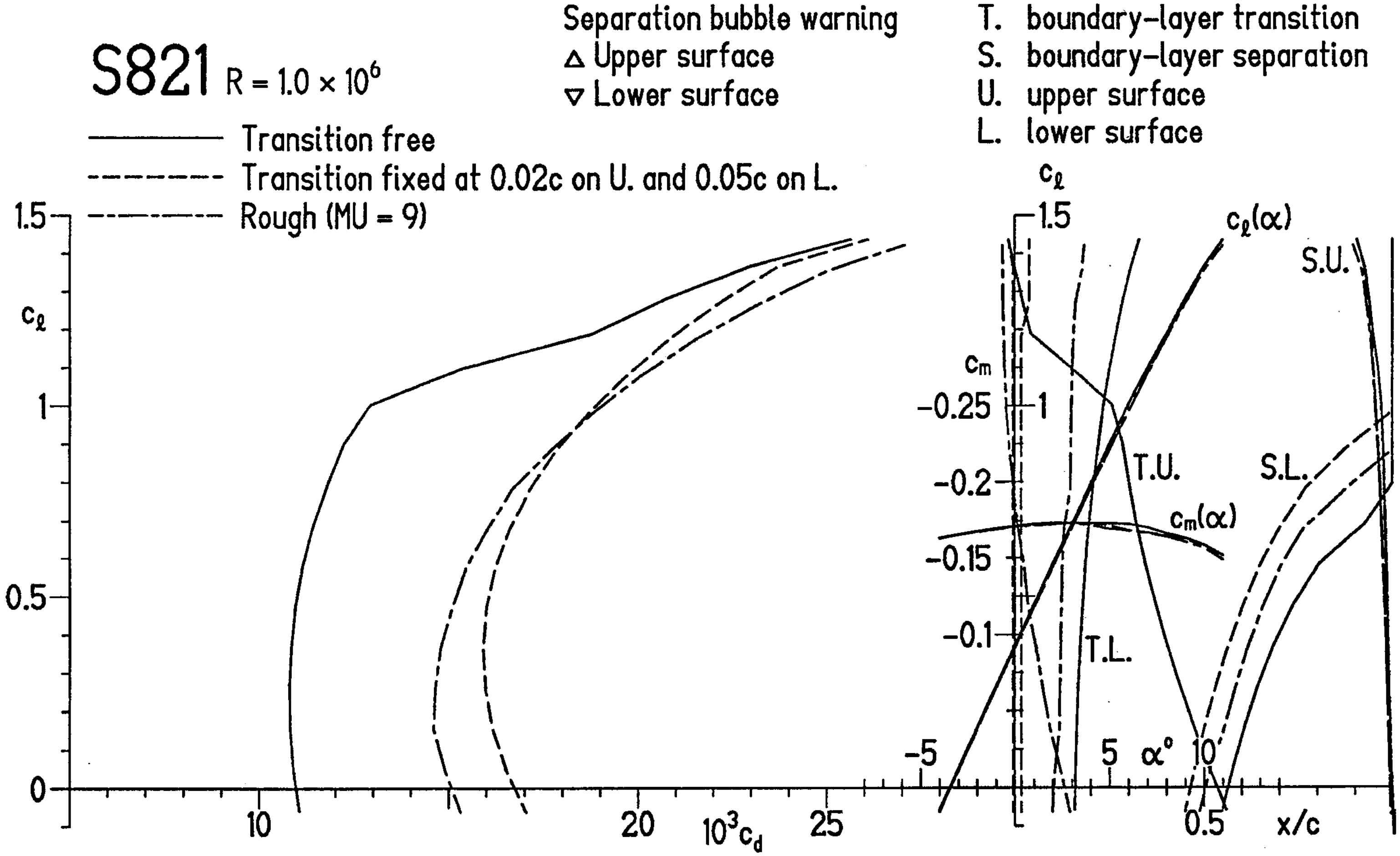

(d) $R = 1.0 \times 10^6$.

Figure 7.- Continued.

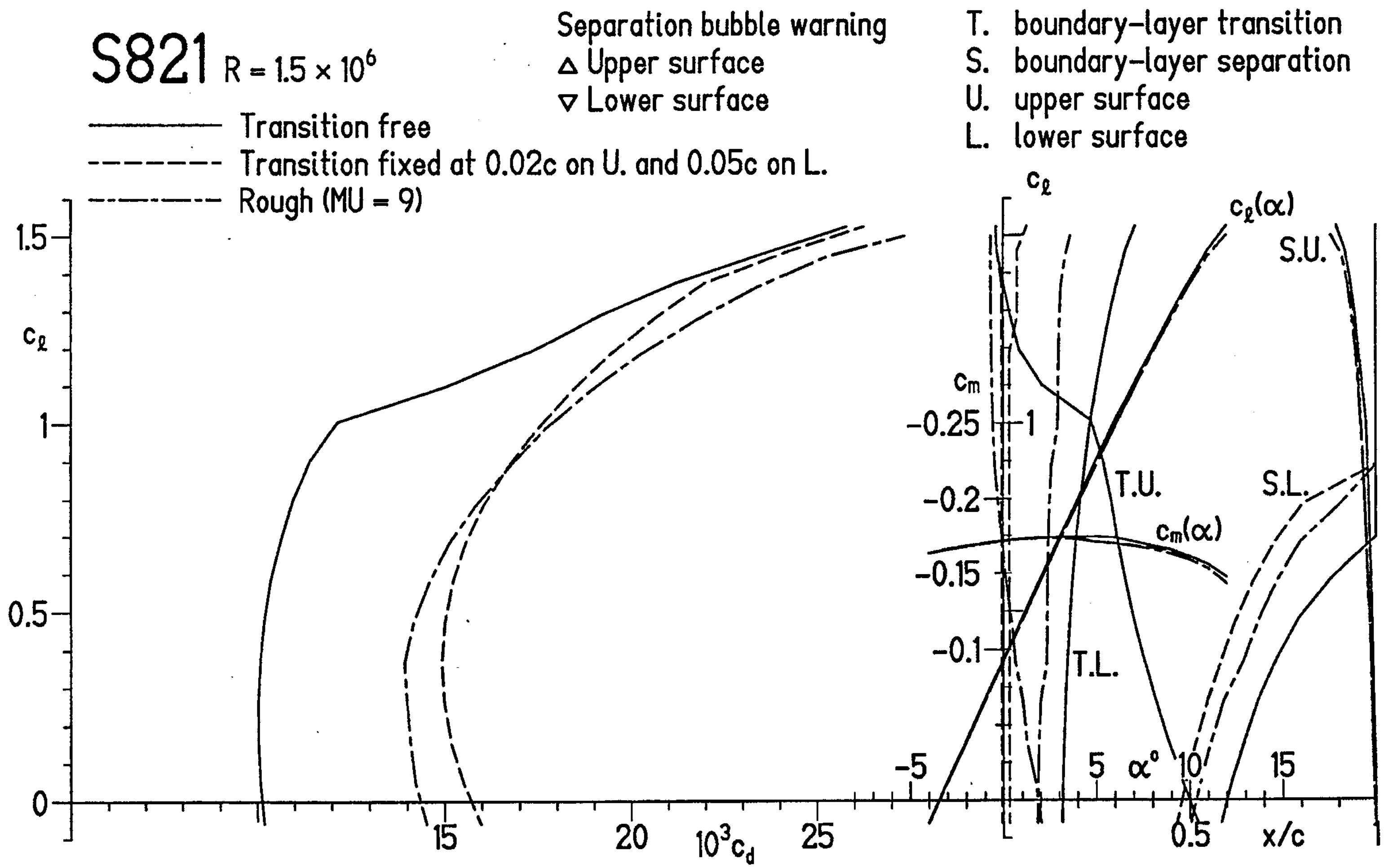

(e) $R = 1.5 \times 10^6$.

Figure 7.- Concluded.

REPORT DOCUMENTATION PAGE	*Form Approved* *OMB No. 0704-0188*

1. REPORT DATE *(DD-MM-YYYY)*	2. REPORT TYPE	3. DATES COVERED *(From - To)*
January 2005	Subcontract report	October 1992 – November 1993

4. TITLE AND SUBTITLE The S819, S820, and S821 Airfoils	**5a. CONTRACT NUMBER** DE-AC36-99-GO10337
	5b. GRANT NUMBER
	5c. PROGRAM ELEMENT NUMBER
6. AUTHOR(S) D.M. Somers	**5d. PROJECT NUMBER** NREL/SR-500-36334
	5e. TASK NUMBER WER4.3110
	5f. WORK UNIT NUMBER
7. PERFORMING ORGANIZATION NAME(S) AND ADDRESS(ES) Airfoils, Inc. 601 Cricklewood Drive State College, PA 16083	**8. PERFORMING ORGANIZATION REPORT NUMBER** AF-1-11154-1
9. SPONSORING/MONITORING AGENCY NAME(S) AND ADDRESS(ES) National Renewable Energy Laboratory 1617 Cole Blvd. Golden, CO 80401-3393	**10. SPONSOR/MONITOR'S ACRONYM(S)** NREL
	11. SPONSORING/MONITORING AGENCY REPORT NUMBER NREL/SR-500-36334

12. DISTRIBUTION AVAILABILITY STATEMENT
National Technical Information Service
U.S. Department of Commerce
5285 Port Royal Road
Springfield, VA 22161

13. SUPPLEMENTARY NOTES
NREL Technical Monitor: J. Tangler

14. ABSTRACT *(Maximum 200 Words)*
A family of thick airfoils for 10- to 20-meter, stall regulated, horizontal-axis wind turbines, the S819, S820, and S821, has been designed and analyzed theoretically. The primary objectives of restrained maximum lift, insensitive tro roughness, and low profile drag have been achieved. The constraints on the pitching moments and airfoil thicknesses have been satisfied.

15. SUBJECT TERMS
airfoils; design; horizontal-axis wind turbines; S819, S820, and S821;

16. SECURITY CLASSIFICATION OF: a. REPORT	b. ABSTRACT	c. THIS PAGE	17. LIMITATION OF ABSTRACT	18. NUMBER OF PAGES	19a. NAME OF RESPONSIBLE PERSON
Unclassified	Unclassified	Unclassified	UL		19b. TELEPONE NUMBER (*Include area code*)

Standard Form 298 (Rev. 8/98)
Prescribed by ANSI Std. Z39.18

F1147-E(05/2004)